# Characterization of Sodium Carboxymethyl Cellulose (Na CMC) Aqueous Solutions to Support Complex Product Formulation – a Rheology and Light Scattering Study

Juliette S. Behra,[†] Johan Mattsson,*[,‡] Olivier J. Cayre,[†] Eric S. J. Robles,[§] Haiqiu Tang,[∥] Timothy N. Hunter[†]

[†]School of Chemical and Process Engineering, University of Leeds, Leeds, LS2 9JT, UK

[‡]School of Physics and Astronomy, University of Leeds, Leeds, LS2 9JT, UK

[§]Newcastle Innovation Centre, Procter & Gamble Company, Whitley Road, Longbenton, Newcastle Upon Tyne, NE12 9BZ, UK

[∥]P&G Technology (Beijing) Co. Ltd, No. 35 Yu'an Road, B Zone, Tianzhu Konggang Development Zone, Shunyi District, Beijing, 101312, China

*k.j.l.mattsson@leeds.ac.uk

## Abstract

Sodium Carboxymethyl Cellulose (Na CMC) is used for its thickening and swelling properties in a wide range of complex formulated products for pharmaceutical, food, home and personal care applications, as well as in paper, water treatment and mineral processing industries. To design Na CMC solutions for applications, a detailed understanding of the concentration-dependent rheology and relaxation response is needed. We address this here by investigating aqueous Na CMC solutions over a wide range of concentrations using rheology as well as static and dynamic light scattering. The concentration dependence of the solution specific viscosities $\eta_{sp}$ could be described using a set of three power laws, as predicted from the scaling theory of polyelectrolytes. Alternatively, a simpler approach could be used, which interpolates between two power law regimes and introduces only one characteristic crossover concentration. We interpret the observed behavior as a transition from the non-entangled semi-dilute to the entangled concentration regimes; this transition behavior was not observed in the solution structure, as determined using static light scattering. Dynamic light scattering revealed three relaxation modes. The two fastest relaxations were assigned as the 'fast' and 'slow' relaxation modes typically

observed in salt-free or not fully screened polyelectrolyte solutions within the semi-dilute concentration range. The third, typically weak mode, was attributed to the presence of a small amount of poorly dissolved cellulose residuals. Since filtration altered the solution behavior, without sufficiently removing the residuals, data collection and processing were adapted to account for this, which facilitated a detailed light scattering investigation of the original solutions, relevant for industrial applications. The relaxation time characterizing the fast mode, $\tau_f$, was concentration independent, whereas the relaxation time of the slow mode, $\tau_s$, demonstrated similar crossover behavior as observed for the specific viscosity, further demonstrating the dynamic nature of the crossover.

**Keywords**

Sodium Carboxymethyl Cellulose (Na CMC); polyelectrolyte; rheology; Dynamic Light Scattering (DLS); Static Light Scattering (SLS).

## 1. Introduction

Sodium Carboxymethyl Cellulose (Na CMC) is a linear semi-flexible negatively charged polyelectrolyte. It is produced from cellulose, the most abundant biopolymer on Earth,[1,2] by substituting some of its hydroxyl groups for carboxymethyl groups.[2-4] Because of its high availability as well as its thickening and swelling properties, Na CMC is widely used in numerous industries.[1,2,5] Application fields include food, pharmaceutical, home and personal-care products, as well paper industry, paint, water treatment and mineral processing.[1,2,5-7] The Na CMC global market represented 1.2 billion USD in 2016[8] and is expected to exceed 1.7 billion USD by 2024.[9]

The market of formulated products (*i.e.* food & beverages, cosmetic & pharmaceuticals, and detergents) represents more than half of the global Na CMC market. Such products contain a large number of compounds such as solid particles (*e.g.* silica), polymers (*e.g.* Na CMC), oils (*e.g.* fragrance and flavoring oils), surfactants, salts or proteins.[10-12] A general challenge in formulating such complex systems is to understand the interactions between the components and their effects on the efficacy and the stability of the product over its shelf-life.

Na CMC is often used in formulated products to control their rheological properties. For example, in the case of toothpaste, Na CMC is responsible for toothpaste performance, including toothpaste stability in its container, dispensing, in-mouth behavior and rinsing of the sink after use.[12] Despite its broad use in industry, Na CMC behavior in solution is still relatively poorly understood and is the subject of research from both fundamental[1,13-16] and applied perspectives.[10,17-20] The polyelectrolyte nature of Na CMC is, in itself, a reason for this poor understanding since many questions remain about the behavior of charged polymers in solution,[16,21] and especially in salt-free solutions; one example concerns the origin of the 'slow' relaxation mode typically observed using Light Scattering (LS), whose presence is not predicted by standard theory.[22-24]

Given the biological origin of Na CMC, it typically has a high polydispersity of the chain length distribution[1,5,25,26] (common values of $M_w/M_n$ are around 1.7-4.5[1,5,13,25,26]). The crystallinity of the cellulose raw material,[3,25,27] and/or the amount and the distribution of the carboxymethyl groups along the chains.[3,19,28-30] can also vary. Commercial Na CMCs typically have an average of 0.4-1.5 carboxymethyl groups per monomer, which is referred to as the absolute Degree of Substitution (DS).[3,19] These charged carboxymethyl groups are key to the behavior of Na CMC in solution as they confer its water-solubility to Na CMC. If there are not enough of these groups and/or if they are not homogeneously distributed along Na CMC chains, Na CMC chains or chain sections are not fully solubilized in water.[3,28,29]

The rheological behavior of Na CMC in water, with or without other compounds (*e.g.* salts,[16,30-33] sugars,[33,34] or surfactants[31,35]), or in solvents such as glycerin/water mixtures,[32] propylene glycol/water mixtures[36] or cadoxen[37] has been characterized. Studies investigating the swelling properties of Na CMC[38] and its ability to form films on its own, or in association with other polymers, have also been performed.[39-41] However, only a few light scattering (LS) studies have been performed on Na CMC solutions, and none, to the best of our knowledge, have been performed on Na CMC solutions without added salt. Several Static Light Scattering (SLS) studies were performed in the 1950-1960s[42-44] on Na CMC in the presence of NaCl and focused on the intrinsic properties of the Na CMC polymer without the effects of charge. Also, four recent light scattering studies that combine LS with other experimental techniques have been published: Dogsa *et al.*[14] studied Na CMC chain conformation as a function of pH while keeping the ionic strength constant at 0.1 M, Guillot *et al.*[35] investigated the behavior of Na CMC in the presence of a surfactant, Hoogendam *et al.*[45] characterized the conformation of Na CMC chains in the presence

of an electrolyte, using Size-Exclusion Chromatography (SEC) coupled to a Multiple Angle Laser Light Scattering (MALLS) detector, and Lopez and Richtering[46] used rheology and DLS to examine the influence of the nature of the counterion on carboxymethyl cellulose behavior.

Generally, both SLS and Dynamic Light Scattering (DLS) have been widely used to characterize polyelectrolytes in aqueous solution. Synthetic polyelectrolytes such as sodium poly(styrene sulfonate) (Na PSS),[47] poly(methacrylic acid) (PMA)[48] or poly(*N*-methyl-2-vinylpyridinium chloride) (PMPVP),[49] as well as natural polyelectrolytes such as DNA,[50,51] chitosan,[52] xanthan[53,54] or hyaluronan[53] have been investigated. For polyelectrolyte solutions above their overlap concentrations, either without added salt or at relatively low salt concentrations so that charges along the chains are not fully screened, DLS typically reveals two relaxation modes: (i) a fast mode which is usually attributed to the coupling between counterions and polyions[49,54] (as the smaller counterions diffuse within the solution, they exert a drag on the oppositely charged polyions) and (ii) a slow mode, whose origin is not fully understood, but is usually attributed to the presence of aggregates or clusters of polyelectrolyte chains, commonly termed 'domains'.[49,54]

The relaxation rate of the fast mode is usually linear in $q^2$ ($q$ is the scattering vector defined as $q = \frac{4\pi n \sin(\theta/2)}{\lambda}$, with $n$ the refractive index, $\theta$ the scattering angle and $\lambda$ the laser excitation wavelength); implying it has diffusive character.[52,53,55-57] The fast mode relaxation time $\tau_f$ is typically around a few μs and the corresponding diffusion coefficient $D_f \sim 10^{-6}$ cm$^2$.s$^{-1}$.[23,58] Detailed discussions about the comparison between predicted and experimental values of $D_f$ can be found in the literature, such as a Sedlák and Amis'[57] about salt-free Na PSS solutions and Topp's about quaternized poly(2-vinylpyridine) in KBr solutions.[59] The slow mode is characterized by significantly longer relaxation times $\tau_s$, that are typically in the range of 1 ms to 10 s.[23,58] The slow mode has commonly been found to also exhibit a linear dependence in $q^2$,[52,53,55-57] for which a diffusion coefficient can be calculated[52] and an apparent hydrodynamic radius of the domains can be estimated.[52] However, other $q$-dependences have been observed for the slow mode[53,57], where it has been suggested that the characteristic size of the domains, $L$, is large compared to the probed length scale so that $qL >> 1$ and internal relaxations within the domains are also probed.[23,58]

To understand the nature of the slow mode, the influence of both the polymer intrinsic properties (*e.g.* $M_w$,[49,53,57] degree of ionization[59-61]) and the experimental conditions (*e.g.* polyelectrolyte concentration,[23,49,53] sample filtration,[23,62] centrifugation,[54,63] dialysis,[60,64] salt addition,[55,60,65]

backbone solvation,[59,65,66] pH[14,60]) have been extensively studied. Nevertheless, there appears to be relatively few outcomes that can be generalized across all the investigated systems. For example, some studies show that, at a given polyelectrolyte concentration, the size of the domains does not vary with $M_w$[49,57] while another shows it does.[53] In a similar way, a study shows that at a given $M_w$, the size of the domains increases with the polyelectrolyte concentration,[23] while others show that it does not.[49,53] However, there does seem to be an agreement on the fact that both filtration and centrifugation can modify the domains.[23,54,62,63] Filtration using small pore size filters can even fully remove them[62,63] or, at least, reduce their size to a level that is below the length scales probed by LS in the particular experiment.[63] Ultracentrifugation has also recently been shown to remove the domains, suggesting that centrifugal forces can break the cohesive interactions in the domains.[54] This observation was suggested to support the idea that the domains result from electrostatic forces and are formed by polyelectrolyte chains sharing counterions.[54] It has also been suggested that they are temporal, in that the polyelectrolyte chains of a domain are continually exchanged with polyelectrolyte chains present in the rest of the solution.[54,55] In some cases, it has been reported that the number of chains forming a domain decreases over long periods of time.[67]

Finally, a third relaxation mode is sometimes observed in polyelectrolyte solutions,[50,58,59,64,67] which is generally either slower than the slow mode[50,59] or situated between the fast and the slow modes.[58,59,67] The reported origin of this relaxation varies significantly between different systems.[50,58,59,64,67] For example, as an intermediate mode, it has been attributed to the motion of polyelectrolyte chain sections that do not belong to the domains,[58] or to the motion of hydrophobic domains formed by uncharged segments of the polyelectrolyte backbone,[59] while as an 'ultra-slow' mode, it has been attributed to loose aggregates of polyelectrolyte chains.[50]

The present work combines viscosity measurements with SLS and DLS over a wide range of polymer concentrations for salt-free aqueous Na CMC solutions. The solution viscosity is studied as a function of polymer concentration. Our results are compared to the predictions of the scaling theory for polyelectrolytes and to recent results from literature; leading to the identification of two concentration regimes and to their assignment to the semi-dilute non-entangled and entangled regimes. Moreover, a comprehensive SLS-DLS study is performed over a similar range of concentrations, where the properties of the excess Rayleigh ratio determined from SLS and the three relaxation modes observed in DLS are investigated.

## 2. Materials and methods

### 2.1. Materials

Na CMC was acquired from Sigma-Aldrich (product number: 419338; lot number: MKBR1032V; manufacturer specifications: average molecular weight 700,000 g/mol and DS 0.8-0.95). We estimated the average molecular weight to $1.2 \times 10^6$ g/mol from the intrinsic viscosity determined with low concentration Na CMC solutions in 0.2 M NaCl (see more detailed explanations in Section 1 of the Supporting Information (SI)). Though larger than the value provided by the supplier, it is identical to the value found by Lopez et al.[16] for a Na CMC with the same product number (*i.e.* the same supplier and specifications). Using the acid wash method from the ASTM,[68] the DS was found to be 0.85 ± 0.03. The moisture content of the polymer powder was 8.4 ± 0.2% (as determined using the method from the ASTM[68]), which was taken into account for the preparation of the polyelectrolyte solutions. 'Ultrapure' water type I (called deionized DI water in the following) was obtained from either a Milli-Q® Advantage A10 ultrapure water station (Merck Millipore) or a PURELAB® Option Q station (Elga). Isopropanol from VWR® Chemicals (AnalaR NORMAPUR® ACS, Reag. Ph. Eur. analytical reagent; product number: 20842.323) and toluene from Fisher Chemical (analytical reagent; product number: T/2300/17) were used.

### 2.2. Methods

#### *2.2.1 Optical microscopy*

Optical microscopy was performed using a Zeiss LSM700 inverted confocal microscope (Carl Zeiss Microscopy) using both phase contrast and differential interference contrast (DIC) techniques.

#### *2.2.2 Rheology measurements*

Initially, stock solutions of 0.037, 0.18, 0.68 and 0.73% Na CMC (all concentrations quoted in this paper are in *wt*%) were prepared by adding the appropriate amounts of Na CMC powder to filtered DI water (using non-sterile Fisherbrand® syringe filters with 0.2 μm pore-size nylon membranes) under stirring with the help of a magnetic stirrer at 850 rpm. Stirring was pursued for 2 h. These initial solutions were diluted to 0.018-0.48% Na CMC and kept overnight before rheology

measurements were carried out. The pH of a few of the Na CMC solutions was measured on the day following sample preparation and was found to be 7.1 ± 0.1, independent of the Na CMC concentration.

All rheology measurements were performed at 25°C using a Discovery HR-2 rheometer (TA Instruments) equipped with a bob and cup geometry (bob with a conical end) on the day following sample preparation. Preliminary measurements of the time-evolution of the viscosity for different constant shear stress values (data not shown) were performed to determine the most suitable shear stress range and time parameters for flow curve acquisition; these include the equilibration time $\Delta t_{eq}$, which is the time during which the shear stress is applied before data acquisition to allow a steady flow to be achieved, and the averaging time $\Delta t_{av}$, which is the time during which data are taken and averaged. All viscosities were measured using the stress-controlled mode. $\Delta t_{eq}$ was set to 200 s for Na CMC concentrations up to 0.18% and to 30 s for all other concentrations. For each solution, flow curve data were collected using $\Delta t_{av}$ = 200 s and $\Delta t_{av}$ = 300 s to confirm that the value of $\Delta t_{eq}$ was adequate and a steady flow had indeed been achieved.

### *2.2.3 Light scattering measurements*

To avoid dust contamination, all glassware were washed with filtered DI water (nylon-membrane filters mentioned in 2.2.2) and filtered isopropanol (non-sterile Fisherbrand® syringe filters with 0.2 μm pore-size PTFE membranes) before being dried in a dust-free environment at *ca.* 50°C. Solutions ranging from 0.018 to 0.92% Na CMC were prepared directly by mixing the appropriate amounts of Na CMC powder and filtered DI water. The preparation procedure was the same as that used for the rheology samples, except that the solutions prepared for LS were transferred into glass vials (rimless Pyrex® culture tubes 75 × 10 mm), suitable for LS, and then kept overnight before the measurements. During the sample preparation tests for the LS measurements, using filtration and/or centrifugation to try to remove contamination (*e.g.* dust), the solutions were filtered using a P5 (1.0-1.6 μm pore size) VitraPOR® Borosilicate 3.3 filter tunnel (ROBU®) before being transferred into LS tubes, and/or centrifuged directly in the LS tubes using a Heraeus™ Megafuge™ 16R Centrifuge (Thermo Scientific™) equipped with a Rotor swing-out TX-400 4 × 400 mL (Thermo Scientific™); both procedures are described in detail in Section 3.3. The reference (*i.e.* toluene) and solvent (*i.e.* water) samples required for excess Rayleigh ratio $\Delta R$ calculations were filtered through previously mentioned PTFE and nylon filters, respectively.

LS measurements were performed at 25.0 ± 0.5°C using a 3D LS spectrometer (LS Instruments, Switzerland) equipped with a HeNe laser ($\lambda$ = 632.8 nm, power: 21 mW), an automated laser attenuator and two avalanche photodiode (APD) detectors. All measurements were performed with vertically polarized incident and vertically polarized detected light and in pseudo-cross correlation mode, which removed after-pulsing effects and allowed the investigation of lag times $\tau$ as low as 25 ns. All samples were transparent and it was confirmed that multiple scattering did not have to be taken into account; thus, all measurements were performed using a standard '2D mode'. The measurements were performed within a few days following solution preparation and did not last more than a week, which is important since Na CMC solution properties such as the viscosity have been shown to change over time.[13,33,69] In the present case, a decrease of *ca*. 7% of the viscosity measured for an applied stress of 0.1 Pa (corresponding to the low shear viscosity plateau) was observed after a week for 0.18% Na CMC solutions, while LS measurements did not show any change after the same ageing time. Further details about the LS measurement process and data analysis are given in Section 3.3.

#### *2.2.4 Fitting of the data*

All fits were performed with Origin® and the Levenberg Marquardt algorithm with 'instrumental weights' was used.

## 3. Results and discussion

### 3.1. Optical microscopy of Na CMC solutions

It became evident upon the initial preparation of the Na CMC solutions that a very small proportion of non-dissolved cellulose residuals remained, even after extended mixing. To understand their nature, we used microscopy and categorized them based upon different observed morphologies, with examples shown in Figure S1 in the SI. The presence of similar residuals in Na CMC solutions was reported as early as 1942 by Höppler.[70] Further investigations on Na CMC samples with a low DS (around 0.7) were performed more recently by Jardeby and co-workers,[29,71,72] who concluded that these residuals were made of non- or poorly-substituted cellulose originating from less reactive cellulose fragments in the raw material used for Na CMC synthesis. Because of their lower DS, these residuals could not undergo full dissolution and would exist in solution as fibers

($DS_{residuals} \approx 0.1$), 'ballooned' fibers ($DS_{residuals} \approx 0.3$-05) or gel particles ($DS_{residuals} \approx 0.5$-0.6).[29] The presence of undissolved residuals in Na CMC solutions for samples with DS values as high as 0.95 has previously been reported.[28,73] In the following, the term 'particulates' will be used for the residuals observed in the studied samples.

Consistent with Jardeby and co-workers's observations[29,71,72], microscopy reveals the existence of particulates as fibers (Figure S1.A), swollen and ballooned fibers (Figure S1.B), or swollen ring-like fragments (Figure S1.C) at more advanced dissolution stages. It is worth noting that studying these particulates using optical microscopy can be difficult. As an example, Figure S2 in the SI shows the same particulates as in Figure S1.C for different *foci*. We also note that similar morphologies to those shown in Figure S1.D were observed in microcrystalline cellulose suspensions, as shown in Figure S3 in the SI; which supports assigning these to non- or poorly substituted cellulose fragments.

### 3.2. Concentration dependence of Na CMC solution viscosity

The scaling model for solutions of uncharged flexible polymers in good solvents classifies their behavior into three concentration regimes: dilute, semi-dilute and concentrated.[74,75] In the dilute regime, the polymer chains are well separated and can be described as a sequence of thermal 'blobs' of size $\zeta_T$*:* for length scales smaller than $\zeta_T$ (*i.e.* within the blobs), the excluded volume interactions are weaker than the thermal energy $kT$ and chains adopt a nearly ideal chain conformation, while for length scales larger than $\zeta_T$, the excluded volume interactions are stronger than $kT$ and the chains can be viewed as self-avoiding walks of thermal blobs.[74] As the semi-dilute regime is entered at the overlap concentration $c^*$, a new length scale, the correlation length $\zeta$, approximately corresponding to the distance between polymer chains and defining so-called correlation blobs, is introduced.[74] At length-scales smaller than $\zeta$, the chain conformations are the same as in the dilute regime, while for length-scales larger than $\zeta$, the excluded volume interactions are screened and each chain can be viewed as a random walk of correlation blobs.[74] As the polymer concentration is further increased, the distance between polymer chains and correspondingly $\zeta$ decrease,[75,76] and when $\zeta$ becomes smaller than $\zeta_T$, the polymer chains behave like ideal chains at all length scales; this is called the concentrated regime[75,76] and the concentration at which it is entered is called $c^{**}$. Moreover, if the polymer molecular weight is high enough, the chains in the semi-dilute and concentrated solutions can be entangled, and the crossover concentration between

the semi-dilute non-entangled and entangled regimes is then called the entanglement concentration $c_e$.

A common method to identify these concentration regimes is to plot the specific viscosity $\eta_{sp}$ (Eq. 1) as a function of the polymer concentration, where $\eta_{sp}$ is defined as:

$$\eta_{sp} = (\eta_0 - \eta_s)/\eta_s \qquad (1)$$

with $\eta_0$ the polymer solution zero-shear viscosity and $\eta_s$ the solvent viscosity. According to the scaling laws for polymer solutions,[16,77] each concentration regime is characterized by a power law $\eta_{sp} \sim c^b$, with a characteristic exponent $b$ that depends not only on the concentration regime, but also on the solvent quality (*e.g.* theta solvent, good solvent).[16,77] For an uncharged flexible polymer in a good solvent, the predicted values of the exponent $b$ for the dilute, the semi-dilute non-entangled, the semi-dilute entangled and the concentrated regimes are 1, 1.3, 3.9 and 3.75, respectively.[16,77]

Importantly, similar concentration regimes have been observed for polyelectrolytes in salt-free solutions.[16,77] The relevant length-scales are here defined by the effects of electrostatic interactions.[21,75] The key length scale of the polyelectrolyte scaling theory[78] is that characterizing so called electrostatic blobs of size $\zeta_e$. Within these blobs, electrostatic interactions are screened and chains act as if they were uncharged, whereas on length-scales larger than $\zeta_e$, the chains adopt stretched directed random walk configurations in the dilute regime due to repulsive interactions between the electrostatic blobs.[1,78] Within the semi-dilute regime, neighboring chains screen electrostatic interactions on length-scales above the correlation length $\zeta$, where chains behave like random walks of correlation blobs.[79] The power law exponent in the dilute regime is predicted to be 1 for salt-free polyelectrolyte solutions, as for neutral solutions, but $c^*$ is typically much lower for polyelectrolyte chains of similar molecular weight due to the significant charge-induced chain stretching.[77] The power law exponents of the semi-dilute non-entangled and entangled regimes are predicted to be 0.5 and 1.5, respectively, while the power law exponent of the concentrated regime should be identical to that observed for neutral polymers (3.75) since the charges of the polyelectrolyte chains are fully screened in this regime.[16,77,79]

Examples of Na CMC solution flow curves spanning the full range of investigated concentrations are shown in Figure S4 in the SI. Flow curves obtained with $\Delta t_{av}$ = 200 s and $\Delta t_{av}$ = 300 s superimposed well (data not shown); which confirms that the time parameters used for the

measurements were appropriate, and the measured viscosities were at steady-state. All solutions are shown to exhibit shear-thinning behavior. The values of $\eta_0$ were obtained by fitting the flow curves with the Carreau model[1] (also shown in Figure S4). The equation as well as the fitting parameters corresponding to the curves shown in Figure S4 are provided in Section 3.1 of the SI. The values of $\eta_0$ were combined with the experimentally determined solvent viscosity $\eta_s = 0.95 \pm 0.06$ mPa.s (see Section 3.1 of the SI) to calculate the specific viscosities $\eta_{sp}$ (Eq. 1), which are shown in Figure 1 as a function of the Na CMC concentration.

For the studied range of Na CMC concentrations, the increase in $\eta_{sp}$ with $c_{Na\ CMC}$ may be described using three different power laws (dashed lines in Figure 1). The determined power law exponents are shown below the fits in Figure 1 and were found to be consistent with those previously reported for other Na CMC solutions.[1,16,80,81] However, a comparison to the exponents theoretically predicted by the scaling theory for polyelectrolytes[15,16] (values in brackets in Figure 1) clearly shows that the exponent value found for the semi-dilute non-entangled regime is higher than the prediction from scaling theory. For their Na CMC samples, Lopez *et al.*[16] obtained a value of 0.68 ± 0.02, similar to our value of 0.71 ± 0.09 within experimental error. They suggested that both polydispersity and chain rigidity could contribute to the discrepancy observed between experimental and predicted power law exponent values in the semi-dilute non-entangled regime.[16] The scaling laws for polyelectrolytes have indeed been established for flexible polymer chains, while it is known that Na CMC polymer chains are semi-flexible.[16,79]

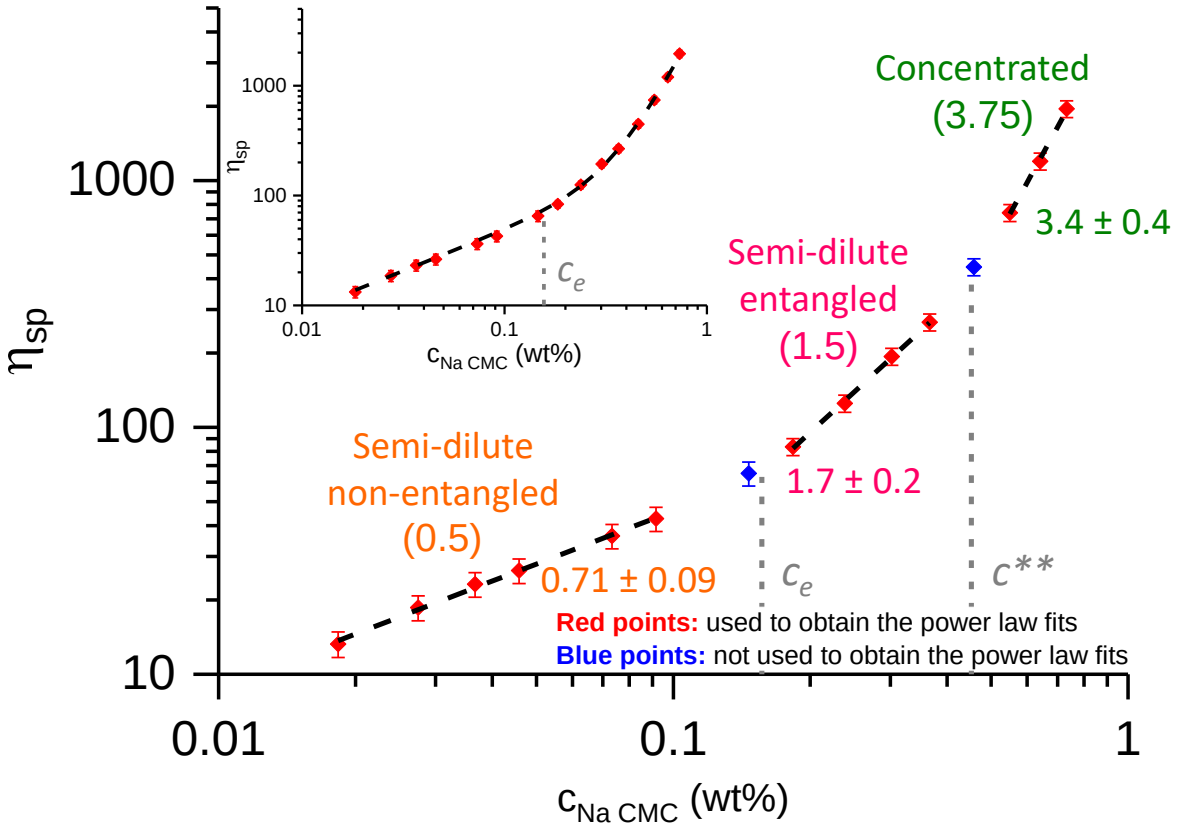


**Figure 1:** Determination of the concentration regimes from the specific viscosity $\eta_{sp}$ *vs* Na CMC concentration $c_{Na\ CMC}$ data. Dashed lines: best power law fits; the corresponding power law exponents are provided below the fitting curves. Theoretical values from the polyelectrolyte scaling laws are given in brackets below the name of each concentration regime. The inset shows the same data set fitted using Eq. 3 where $b$ = 0.71 and $c_e$ = 0.16 *wt*% (values obtained from the best power law fits). The fit with the power law exponent predicted by the scaling law is shown in Figure S5.

The crossover concentrations are shown in Table 1. It is worth noting that as non-fractionated Na CMC samples are generally polydisperse,[1] we expect the transitions between different concentration regimes to be characterized by a concentration range instead of a single characteristic concentration. Thus, the concentrations determined using the power law fitting approach should be viewed only as estimates. Because the exponents of the best power law fits are different from those predicted by the scaling laws, the crossover concentrations $c^*$, $c_e$, and $c^{**}$, calculated as the intersections between the power law fits of two successive concentration regimes, differ depending on whether theoretical or best fit exponents are considered (*i.e.* upper and lower lines of Table 1 respectively). The fits of the semi-dilute non-entangled concentration regime obtained with both theoretical and best fit exponents were extrapolated to $\eta_{sp}$ = 1 to obtain the values of the overlap concentrations. These processes are illustrated in Figure S3.

**Table 1:** Crossover concentrations calculated with different methods.

| Calculation method | $c^*$ (*wt*%) | $c_e$ (*wt*%) | $c^{**}$ (*wt*%) |
|---|---|---|---|
| Scaling law fits | $7.1 \times 10^{-5}$ | 0.11 | 0.46 |
| Best power law fits | $4.7 \times 10^{-4}$ | 0.16 | 0.45 |

By studying how the crossover concentrations and the specific viscosity behave with Na CMC molecular weight, Lopez *et al.*[1,16] concluded that the scaling laws of salt-free polyelectrolyte solutions may not be the most appropriate model to describe salt-free Na CMC solutions above $c^*$. Their study[16] indicated that there may be only one crossover concentration, instead of the two separate concentrations, $c_e$ and $c^{**}$. This hypothesis was reinforced by the absence of the expected change in the Small Angle Neutron Scattering (SANS) profile at $c^{**}$, which suggests that the current description of such systems based on the electrostatic blobs and the correlation length is not sufficient to describe them,[1] as well as by the fact that viscosity data could be successfully fitted outside the dilute regime using a simple expression (Eq. 2) that contains only one characteristic concentration within the fitting regime, chosen as the entanglement concentration $c_e$ determined as discussed above. Eq. 2[16] is a simple parameterization of the $\eta_{sp}$ *vs* $c_{Na\ CMC}$ data above $c^*$, which uses a single characteristic concentration $c_e$ outside the dilute regime and includes two parameters $\gamma$ and $q$ to describe the power law exponents in the non-entangled and entangled regimes. To account for variations in the shape of $\eta_{sp}$ *vs* $c_{Na\ CMC}$ as the behavior transitions from the low to high concentration power law behavior, a final parameter $Q$ is introduced.

$$\eta_{sp} = \eta_{sp}(c^*) \cdot (c_{Na\ CMC}/c^*)^{\gamma} \cdot (1 + Q(c_{Na\ CMC}/c_e)^q) \qquad (2)$$

An attempt to fit our data outside of the dilute regime with Eq. 3, adapted from Eq. 2 to avoid any assumption on the values of $\eta_{sp}(c^*)$ and $c^*$, is shown in the inset to Figure 1. Here $\gamma$ is the exponent of the best power law fit within the semi-dilute non-entangled regime (*i.e.* $\gamma$ = 0.71), $c_e$ is the entanglement concentration determined from the scaling law analysis described above (see value in Table 1), and $A$, $Q$ and $q$ are fitting parameters.

$$\eta_{sp} = A \cdot c_{Na\ CMC}{}^{\gamma} \cdot (1 + Q(c_{Na\ CMC}/c_e)^q) \qquad (3)$$

The fit is also shown in Figure S3 of the SI, where it is compared to that using the exponent predicted from scaling theory (*i.e.* $\gamma$ = 0.5) and where all parameters are provided for both fits. Eq. 3 is found to fit the data well, which supports the possibility that there may be only one

crossover concentration above the overlap concentration. It is worth noting that the existence of the concentrated regime has also been questioned for another polyelectrolyte system by Dou and Colby.[78] While the graph of $\eta_{sp}$ *vs* $c_{polymer}$ was consistent with the scaling law predictions, the concentration-dependence of the terminal modulus *G* did not show the expected inflection at *c***.

In summary, a detailed analysis of the concentration dependence of the specific viscosity has been performed above the overlap concentration. Our data can be described using a set of power laws as predicted from the scaling laws for polyelectrolytes. The determined power law exponents slightly differ from the theoretical predictions, but are consistent with those previously determined for Na CMC samples of varying $M_w$ and DS.[1,15,16] Importantly, we can alternatively describe the same data using a simpler approach which interpolates between a low and a high concentration power law behavior using only a single crossover concentration. This concentration is assigned to that characterizing the onset of entanglements within the semi-dilute regime.

### 3.3. Optimization of light scattering measurements

LS measurements are very difficult to perform for Na CMC concentrations below 0.018% due to the low scattering intensity. It was thus decided to limit the LS study to Na CMC concentrations starting from 0.018% and covering the concentration range investigated with viscosity measurements (see Section 3.2).

*Sample preparation*

LS measurements ideally require samples free of dust and residual components.[60,82] Observations of the Na CMC solutions using optical microscopy, however, showed the presence of particulates (see Figure S1 in the SI). Thus, the possibility of removing these particulates from the solutions prior to performing the LS measurements was investigated. Filtration and centrifugation are the two most commonly used techniques for this purpose.[14,60,82] 0.2 μm pore-size syringe filters were tried first. However, the scattering intensities of the Na CMC solutions after filtering using such filters were very close to those of pure water (data not shown). This result clearly demonstrated that these filters are not appropriate for sample preparation, which is consistent with the fact that the characteristic diameter of the 'domains' responsible for the slow relaxation mode scattering contribution was determined to be around 400 nm (see Section 3.5, and Figure S24 in the SI).

Jardeby and co-workers have previously isolated particulates from Na CMC solutions (see Figure S1 and Jardeby and co-workers' papers[29,71,72]) using filters, and the same filter types (*i.e.* ROBU® VitraPOR® Borosilicate 3.3 filter tunnels) were thus tried in the present study, using the smallest available pore size (1.0-1.6 μm). Centrifugation tests were also carried out, and were performed directly in the LS cells to prevent any contamination of dust due to the sample transfer into the cells.[60] The centrifugation acceleration and deceleration speeds were set to the lowest available values to minimize any modification of the solution structure.[60,63] For the same reason, the Relative Centrifuge Force (RCF) and the centrifugation times were varied to ensure that none of the chosen values modified the solution behavior significantly, as several studies have shown that centrifugation can alter the solution properties.[54,58] Both the filtration and centrifugation trials were performed on 0.018% Na CMC solutions. The effectiveness of these preparation protocols to remove dust and residual components were evaluated using LS. The intensity auto-correlation data corresponding to a range of different preparation protocols are shown in Figure 2.

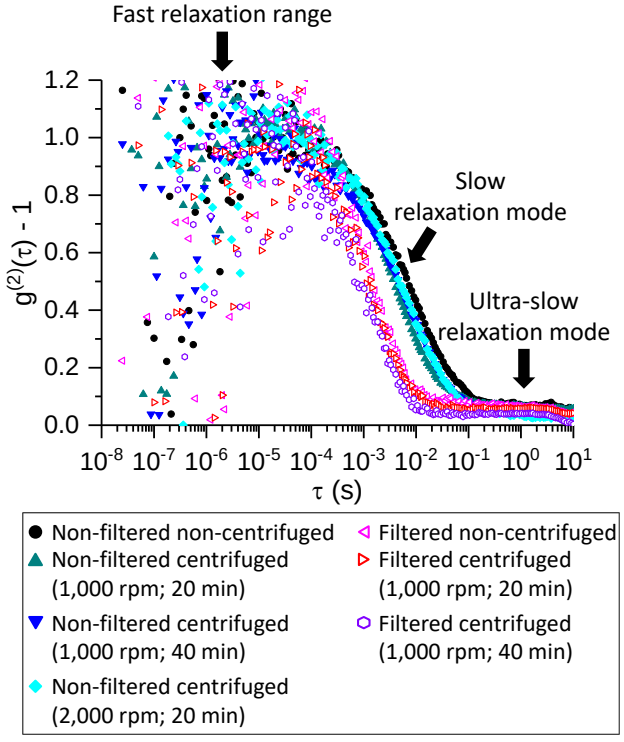


**Figure 2:** Normalized intensity auto-correlation data at 90° scattering angle collected during sample purification trials (*i.e.* centrifugation and/or filtration) for a 0.018 *wt*% Na CMC solution. Each data series is an average of 30 s measurements (See details about normalization and averaging in Section 4.3 of the SI.)

All intensity auto-correlation data exhibit two decays: (i) a main decay with a relaxation time around either 0.01 s or 0.003 s, and (ii) a secondary decay at much longer relaxation times. The main relaxation (i) was assigned to the slow relaxation normally reported for salt-free polyelectrolyte solutions above $c^*$, and thought to be due to the presence of polyelectrolyte aggregates here termed 'domains',[55,83] as discussed in the introduction. None of the investigated centrifugation parameters modified the value of the relaxation time $\tau_s$ of the slow mode significantly, which demonstrates that the behavior of the Na CMC solutions was not altered by the centrifugation procedure. Conversely, filtration led to a significant decrease in $\tau_s$, suggesting that the compositions and/or the structures of the solutions were considerably modified. This observation is in agreement both with previous literature on light scattering of salt-free polyelectrolyte solutions[23,63] and with an observed 12.2 ± 0.6% decrease of the viscosity upon filtration (data not shown). The origin of the secondary decay, referred to here as the ultra-slow mode, is not clear. The corresponding relaxation times are long, suggesting that the ultra-slow mode is due to the presence of large particulates present in solution (see 3.5 for a more detailed discussion). As neither centrifugation nor filtration completely removed the ultra-slow mode, and filtration even significantly altered the slow relaxation mode-, the LS measurements were performed using unprocessed Na CMC solutions. The next two sub-sections describe how data collection and processing were adapted to account for the presence of the ultra-slow mode. Importantly, our approach has the clear advantage that it allowed detailed light scattering measurements to be performed on the original Na CMC solutions which are relevant for industrial applications.

*Measurement settings*

For each solution, preliminary measurements at different angles were performed to identify the most appropriate measurement durations. DLS measurements need to be long enough so that the determination of the intensity auto-correlation data is reliable. However, particularly for the lower concentration range, where the scattering is weak, the acquisition times that can be used are limited since scattering from particulates (assumed to be responsible for the ultra-slow mode) will eventually interfere with the scattering from the Na CMC solution. This is demonstrated in Section 4.1 of the SI, where Figure S6 shows both DLS and SLS data collected for different durations on a 0.018% Na CMC solutions.

From a practical viewpoint, more but shorter measurements can be performed at each scattering angle so that measurements that are significantly impacted by scattering from particulates can be discarded. Subsequently, the remaining data are averaged across several independent measurements to enable good statistics for samples at low concentrations, where the intrinsic scattering is low, without significant effects of scattering from particulates.

*Data processing*

The LS data need to be collected within the linear range of the detector to be reliable. As a consequence of the presence of particulates in the solutions, extra precautions were required to make sure this condition was always met, as explained in detail in Section 4.2 of the SI. Hence, the first data processing step was to remove all measurements during which the scattering intensities were outside the detector linear range, which occurred for some experimental runs influenced by the stronger scattering contribution from particulates. Subsequently, the scattering traces (*i.e.* scattering intensity over time) were investigated and traces which contained clear contributions to the scattering from particulates, as identified by sharp peaks with significantly higher intensity than the intensity fluctuations corresponding to the contributions from the intrinsic solutions, were removed. This trace check was performed for all DLS measurements, while it was only performed for the measurements where the scattering was far above the mean for SLS data.

The obtained SLS data were used to calculate the excess Rayleigh ratio $\Delta R$ using Eq. 4[84]

$$\Delta R(\theta) = \frac{I_{norm,sample}(\theta) - I_{norm,water}(\theta)}{I_{norm,toluene}(\theta)} \left(\frac{n_{sample}}{n_{toluene}}\right)^2 R_{toluene} \qquad (4)$$

where $n_{sample}$ and $n_{toluene}$ are the measured sample refractive index and the toluene refractive index respectively, $R_{\text{toluene}}$ is the Rayleigh ratio of toluene at $\lambda$ = 632.8 nm, and $I_{norm} = \frac{measured\ count\ rate \times sin(\theta)}{laser\ intensity}$.

For DLS on the solutions with low polymer concentration (0.018-0.073%), the intensity auto-correlation data from multiple experimental runs were averaged to obtain the final intensity auto-correlation curves. The data processing methodology is summarized in Figure S8 of the SI.

The way of fitting the data depended on the Na CMC concentration, and examples of fitting approaches are shown in Figure S9 for solutions of low (0.018-0.073%), intermediate (0.18-0.37%) and high (0.55-0.92%) Na CMC concentrations. Eq. 5[14,83] could be used to fit all the

intensity auto-correlation data, where *f*, *s* and *us* refer to the fast, slow and ultra-slow mode respectively, $A_i$ is the amplitude of the mode *i*, $\beta_i$ is the stretching coefficient of the mode *i* and $\tau_{e,i}$ is an effective relaxation time of the mode *i*. The average relaxation time $\tau_i$ of the mode *i* is linked to $\tau_{e,i}$ with $\tau_i = \frac{\tau_{e,i}}{\beta_i}\Gamma\left(\frac{1}{\beta_i}\right)$ where Γ is the gamma function.[14,83]

$$g^{(2)}(\tau) - 1 = \left[A_f e^{-(\frac{\tau}{\tau_f})} + A_s e^{-(\frac{\tau}{\tau_{e,s}})^{\beta_s}} + A_{us} e^{-(\frac{\tau}{\tau_{e,us}})^{\beta_{us}}}\right]^2 \qquad (5)$$

The fast mode could not be observed for the least concentrated solutions (Figure S9.$A_2$), so here $A_f$ was set to 0 and only the slow and the ultra-slow modes were fitted. For the high Na CMC concentrations, it was not possible to get a satisfactory fit with Eq. 5. Therefore, the contributions of the fast and the slow modes were determined using two different fits as detailed in Section 4.3 and Figure S8 of the SI, and illustrated in Figures S9.$C_2$ and S9.$C_3$. The residuals of the fits shown in Figure S9 are displayed in Figure S10 of the SI and demonstrate that the data are successfully fitted using the approach described above. The fitting of the fast mode is further commented in Section 4.4 of the SI.

### 3.4. Static light scattering measurements

The excess Rayleigh ratio $\Delta R$, calculated from SLS data, is plotted as a function of scattering wave-vector *q* in Figure 3.A. $\Delta R$ increases with increasing Na CMC concentration and decreases with increasing *q*, following an approximate power law relationship (see dashed lines in Figure 3.A). At low *q* and high $c_{Na\ CMC}$, the data points are more scattered and fall above the power law fits; the likely reason for this behavior is the presence of the sample particulates which provide an additional scattering contribution that is most prominent at small scattering angles. The power law exponent values obtained from the data fitting are shown in Figure 3.B for samples of varying Na CMC concentrations. No significant concentration dependence of the power law exponents is observed, and their average value across the concentration range is estimated as -2.36 ± 0.05. It is worth noting that this value is, within the experimental error, identical to the one determined from the contribution of the slow relaxation mode – attributed to the domains – to the excess Rayleigh ratio $\Delta R_s$ (see Sections 4.6.1 and 4.6.3 of the SI about $\Delta R_s$) as shown in Figure 3.B. Similar values have been observed for other polyelectrolytes such as PMPVP[49] ($d_f$ = 2.2 ± 0.2) or poly(*N*-benzyl-2-vinylpyridinium bromide)[55] ($d_f$ = 2.7). This power law exponent has sometimes been interpreted

as the fractal dimension of the system. However, given the relatively small *q*-range and the fact that observing an approximate power law does not necessarily indicate a fractal behavior, this interpretation must be considered with care. In addition, Zhang *et al.*[85] have shown that the value of the exponent for a polyelectrolyte can vary significantly depending on the experimental conditions (*e.g.* solvent nature) and suggested that the structure of the domains is not universal.

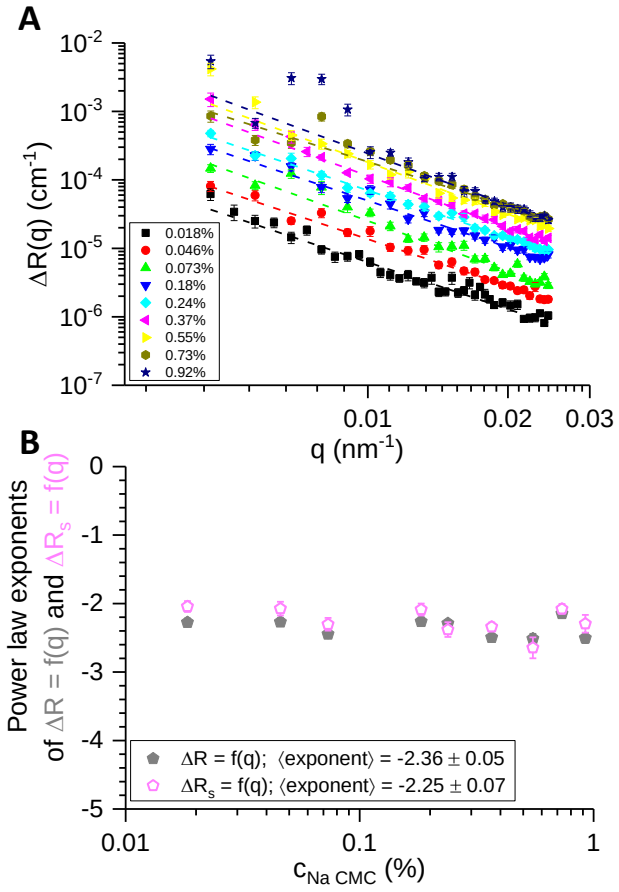


**Figure 3:** *q*- and $c_{Na\ CMC}$-dependence of the excess Rayleigh ratio $\Delta R$. **A.** Excess Rayleigh ratio $\Delta R$ as a function of the scattering vector *q* for all the studied concentrations. The dashed lines are power law fits. **B.** Exponents resulting from both the power law fits shown in A (full grey symbols), and the power law fits of the slow relaxation mode contribution to the excess Rayleigh ratio $\Delta R_s$ (empty pink symbols; the data $\Delta R_s = f(q)$ are plotted in Figure S18.A). In both A and B, $c_{Na\ CMC}$ is in *wt*%.

Moreover, the power law exponent can be compared to the power law exponents determined by Lopez and co-workers[1,15] for the low *q* upturn observed in their SANS experiments, where the value of the exponent was DS-dependent. For solutions made with a Na CMC of similar DS but lower $M_w$ (DS = 0.8 ± 0.1; $M_w = 3.1 \times 10^5$ g/mol) than the one studied here, the power law exponent describing the low *q* upturn was -3.4 at low Na CMC concentrations (4-8 g/L ~ 0.4-0.8%), and -1

at higher concentrations (20-28 g/L ~ 2-2.8%).[15] Our value of -2.4 thus lies between these two values. It is worth noting that direct comparison between Lopez *et al.*'s data[15] and ours should be carried out with caution since the Na CMC molecular weights are different and, even if the their lower investigated concentrations overlay with the higher concentrations investigated here, solution structure and dynamics may be different as the crossover concentrations are different.[16] Assuming that both the low $q$ upturn observed by SANS and the SLS profile probe the same structural features, the difference observed between Lopez *et al.*'s power law exponents[15] and ours could arise from the difference in $M_w$ between the two Na CMCs; the domain size has been shown to be $M_w$-dependent in a number of previous studies on high $M_w$ polyelectrolytes.[53,55,57,86] The differences could also be explained by the fact that different length scale ranges are probed in these experiments. Indeed, our investigated $q$ range is 0.005-0.024 $nm^{-1}$, while the one investigated by Lopez and co-workers[1,15] corresponds to $q$ values above 0.04 $nm^{-1}$. Hence, a difference between the power law exponent determined within the $q$ range probed by SLS, compared with that probed within the low $q$ range probed by SANS, was reported by Borsali *et al.*[50] for DNA solutions. Furthermore, to achieve enough scattering contrast, Lopez and co-workers[1,15] studied their Na CMC solutions in $D_2O$ rather than in $H_2O$ and the structure of Na CMC solutions might be different in non-deuterated and deuterated aqueous solutions. Even though many properties of both $D_2O$ and $H_2O$ are similar, the hydrogen bond strength is slightly different,[87] and as an example, SLS experiments performed with guar, a neutral polymer, show that both the scattering intensity and the power law exponents describing $\Delta R = f(q)$ are higher in $D_2O$ compared to $H_2O$. Gittings *et al.* [88] suggest that, in the case of guar, the observed difference is due to the poorer solubility of guar in $D_2O$ compared to $H_2O$.[88]

To determine the excess Rayleigh ratio in the zero wave-vector limit $q = 0$, $\Delta R(0)$, Zimm plots ($[K.c_{Na\,CMC}/\Delta R] = f(q^2)$ where $K$ is an optical contrast constant[89] (see Eq. S3 in the SI)) were produced, for which an example is shown in Figure S13.A. However, for most of our solutions, the $q = 0$ intercepts were slightly negative, which indicates the presence of excess scattering at low $q$ and thus the presence of large structures.[89] Berry ($[K.c_{Na\,CMC}/\Delta R]^{0.5} = f(q^2)$)[89] and Guinier ($\ln[K.c_{Na\,CMC}/\Delta R] = f(q^2)$)[89] plots were also considered as they might be more successful at linearizing the data at low $q$ values[89] and examples are shown in Figure S13. As the linear part covered a wider range of $q$ values for Berry plots as compared to Guinier plots, further calculations were performed with the data obtained from the Berry plots. Ioan *et al.*[83] obtained similar Berry

plots for dextran solutions above *c**. It is also worth noting that, as shown in Section 4.6.3 of the SI, the same behavior was observed for the proportion of the excess Rayleigh ratio corresponding to the slow mode; which suggests that the observed behavior of the total excess Rayleigh ratio is mainly driven by the domains responsible for the slow mode.

The obtained values of *ΔR(0)*, as well as the values of *ΔR* at different angles, are plotted as a function of Na CMC concentration in Figure 4. For each angle, the data $\Delta R = f(c_{Na\ CMC})$ were fitted using power laws (dashed lines in Figure 4), and the power law exponents for all angles were found to be $0.91 \pm 0.02$. Sedlák and Amis obtained similar results, though their power law exponents were slightly above 1.[47]

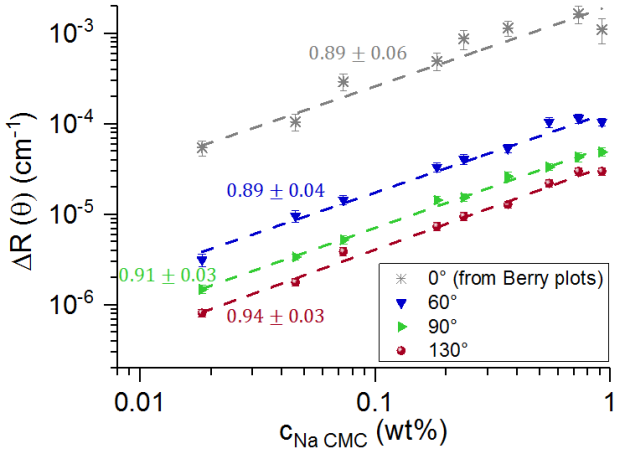


**Figure 4:** Concentration dependence of the excess Rayleigh ratio *ΔR(θ)* at different angles. The values of the excess Rayleigh ratios at 0° (or $q = 0$) were obtained by linear extrapolation of the Berry plots at low *2* values. Dashed lines are power law fits whose exponent values are provided next to each fit.

In conclusion, we found that $\Delta R \sim q^{\alpha}$ across the investigated concentration range with a concentration-independent power law exponent $\alpha = -2.36 \pm 0.05$. We also found that $\Delta R(\theta) \sim c_{Na\ CMC}{}^{\alpha'}$ with a consistent power law exponent $\alpha' \sim 0.9$. Thus, from SLS, we do not find any evidence for a change in structure across our investigated concentration range.

### 3.5. Dynamic light scattering measurements

Examples of normalized intensity auto-correlation data at different scattering angles for two solutions, illustrating the behavior observed at low (0.018-0.073%), and higher (from 0.18%) Na CMC concentrations, are shown in Figures 5.A and B, respectively. For each solution, the characteristic relaxation time of the slow mode is shifted towards longer times as the scattering

angle decreases.[55] However, for some data sets, the amplitude of the ultra-slow mode is significant; particularly for the two lowest scattering angles shown in Figure 5.B. To address this issue, we take account of the ultra-slow mode in the fitting procedure, as described in Section 3.3, and Figure S8 of the SI. Also, as discussed previously (Section 3.3), the fast mode cannot be observed for the least concentrated solutions, despite their concentrations being above the overlap concentration $c^*$, which is likely due to it being hidden in the noise observed at low lag times $\tau$. When the fast mode can be observed (at higher concentrations) its relative amplitude (compared to the slow mode) increases for increasing scattering angles.[55] This is explicitly shown in Figure S14 of the SI and agrees with the commonly observed behavior for polyelectrolytes.[52,53] Figure S14, however, also shows that the relative amplitude of the fast mode is concentration-independent, which is different from the behavior reported for some polyelectrolytes.[52,53,55,56]

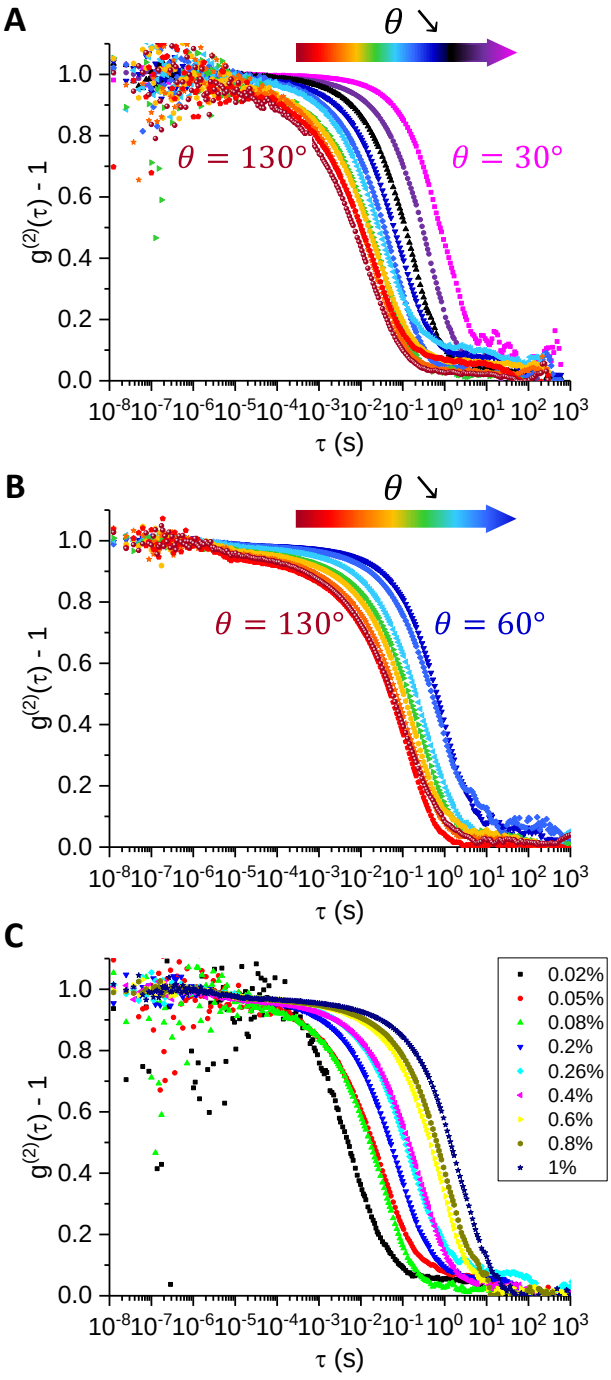


**Figure 5:** Influence of the scattering angle $\theta$ and Na CMC concentration on the normalized intensity auto-correlation data. **A. B.** Data collected for a wide range of angles in steps of 10° on the 0.073 *wt*% (low concentration) and the 0.37 *wt*% (intermediate-high concentration) Na CMC solutions, respectively. **C.** Data at 90° scattering angle for all the investigated Na CMC concentrations ($c_{Na\ CMC}$ in *wt*%). These data are also shown in Figure S16 of the SI with data collected at 60° and 130°. The data are averaged intensity auto-correlation data for 0.018, 0.046 and 0.073 *wt*% Na CMC, while they are angle-representative curves for all the other Na CMC concentrations. In A and B, the step between two successive angles is 10.

Intensity auto-correlation data for each solution are compared at 90° in Figure 5.C. The relaxation time of the fast mode is concentration-independent.[55,56] The relaxation time of the slow mode, conversely, increases across the concentration range.[55,56]

*Ultra-slow mode*

The ultra-slow mode is characterized by a long relaxation time and was present in all solutions at all scattering angles. Moreover, neither filtration nor centrifugation were able to remove this decay to a significant degree (see Section 3.3). As mentioned in Section 3.3, the presence of particulates in the Na CMC solutions (see Figure S1 of the SI) could explain the presence of the ultra-slow mode. The size of the smallest particulates determined by optical microscopy (Figure S1.C) is in the range of 1-10 μm, but difficulty in determining the size using optical microscopy made exact size determination difficult (see Section 3.1). While the smallest particulates could pass through the glass filter (pore size: 1.0-1.6 μm), some larger particulates may also go through if they have the ability to deform and change shape during filtration. Assuming the diffusion of these 1-10 μm-diameter particulates solution is Brownian in the 0.018% Na CMC solution and the viscosity they experience is that of the solution (see Eq. 8), the corresponding relaxation times at a scattering angle of 90° would be in the range of 0.09-0.9 s, while they would be in the range of 12-120 s for the 0.73% Na CMC solution under the same hypotheses. For both Na CMC concentrations, these relaxation times are longer than the relaxation times of the slow mode, but smaller than those observed for the ultra-slow mode (Figure 5.B). The assumptions behind this simple argument, including simple Brownian motion, a spherical particle shape and the fact that the particulates experience the viscosity of the solution are most unlikely to be all true. Even more likely, the strong contribution to the resulting scattering of the largest particulates, such as the fiber shown in Figure S1.A, would, in effect, hide the contribution from smaller particulates, and result in the very long relaxation times we observe.

The amplitude of the ultra-slow mode was typically higher for lower Na CMC concentrations (see Figure 5.B and Figure S16 in the SI), which is reasonable since, at low Na CMC concentrations, the scattering of the Na CMC solutions themselves would be very weak and we would thus observe the particulates to a greater degree. In addition, these solutions have lower viscosities, meaning that particulates would move faster and their scattering is more likely to be detected within the set acquisition time. Moreover, the values of the ultra-slow mode fitting parameters vary significantly

between repeat measurements, which strongly suggests that the ultra-slow mode relaxation time is too long compared with measurement durations to collect statistically reliable data for this mode. Thus, the fitting of the ultra-slow mode was only used to effectively remove its contribution from the results of the two other modes, and the corresponding fitting parameters have not been included.

*Fast mode*

The contribution of the fast mode to the total excess Rayleigh ratio $\Delta R_f$ (called fast mode amplitude by Sedlák[63]) is $q$-independent within experimental error as shown in Figure S16 of the SI and is proportional to the Na CMC concentration. A similar $q$-independence of $\Delta R_f$ was found for Na PSS in an organic solvent, *N*-methylformamide, and in the presence of various amounts of NaCl[65] as well as for poly(acrylic acid) (PAA) in water.[60]

The $q$- and $c_{Na\ CMC}$-concentration dependences of the fast relaxation time $\tau_f$ are shown in Figure 6. The curves of $\tau_f = f(q)$ superimpose well within the experimental error for all the studied solutions, which confirms that the fast-mode is independent of Na CMC concentration (as discussed in relation to Figure 5.B). The $q$-dependent data can be fitted by a power law with an exponent value of 2.5 ± 0.3. This is close to the usually reported value of 2,[52,53] and characteristic for a diffusive process; this small discrepancy is thought to be due to the difficulties encountered in the fitting of the fast mode (see Section 3.3).

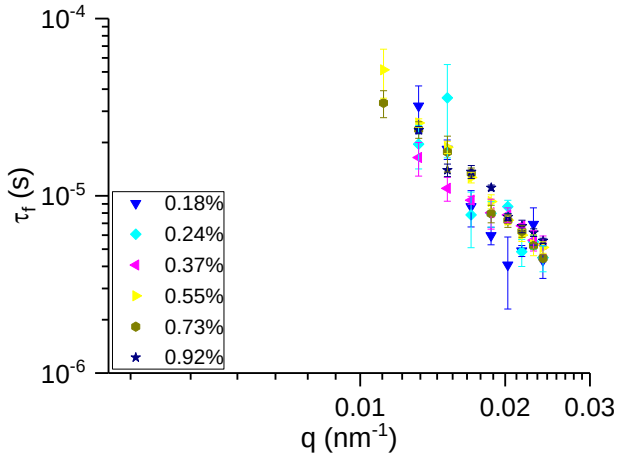


**Figure 6:** $q$- and $c_{Na\ CMC}$-dependences of the fast mode. Fast relaxation time $\tau_f$ as a function of the scattering vector $q$ for solution concentrations of 0.18 *wt*% Na CMC and above ($c_{Na\ CMC}$ in *wt*%). The curves were fitted with power laws which are not represented for clarity. The average exponent across all concentrations is -2.5 ± 0.3.

Considering the fast mode as a diffusive process, attempts were made to calculate the fast mode diffusion coefficient $D_f$. The different methods used are explained below and further illustrated in Figure S17 in the SI. For each solution, the data $\tau_f^{-1} = f(q^2)$ were fitted using Eq. 6.

$$\tau_f^{-1} = A + D_f q^2 \qquad (6)$$

where $A$ is the intercept of the linear curve and is either set to be free or set to 0. Eq. 6 with $A = 0$ is expected for simple diffusive behavior[50,82] while Eq. 6 with $A \neq 0$ accounts for a small uncertainty in the determined values of $\tau_f$ (see Section 3.3). As shown in Figure 7, which displays the values of $D_f$ obtained using different calculation methods, the two methods used to determine $D_f$ lead to consistent results within the accuracy of the data. Two other calculation methods were also investigated: $D_f$ values were computed at each angle with $D_f = \tau_f^{-1} q^{-2}$ (equivalent to Eq. 6 with $A = 0$)[57] before being fitted as a function of $q^2$ with Eq. 7 for $B = 0$ and $B \neq 0$.

$$D_f = D_f(q^2 = 0) + Bq^2 \qquad (7)$$

The results of these calculations are also shown in Figure 7. The values of $D_f$ obtained from all four calculation methods are close to each other and are of the same order of magnitude as those generally observed for other polyelectrolytes[51,57,85,90] (*i.e.* around $10^{-6}$ cm$^2$.s$^{-1}$). A value of $D_f$ of $(3.1 \pm 0.2) \times 10^{-6}$ cm$^2$.s$^{-1}$ is obtained using Eq. 6 with $A = 0$ and Eq. 7 with $B = 0$; which are the simplest methods and correspond to what is expected for diffusive behavior. This value is similar to the value of $4.9 \times 10^{-6}$ cm$^2$.s$^{-1}$ reported by Lopez and Richtering[46] for a 0.2 *wt*% Na CMC solution prepared with a Na CMC of smaller $M_w$ and higher DS; thus showing the independence of $D_f$ from $M_w$ and DS. This finding is also consistent with that of Sedlák and Amis,[47] who showed that $D_f$ was independent from $M_w$ for sodium poly(styrene sulfonate), as well as with that of Förster *et al.*,[55] who reported $D_f$ to be independent from both the degree of quaternization and the molecular weight for quaternized poly(vinyl pyridine).

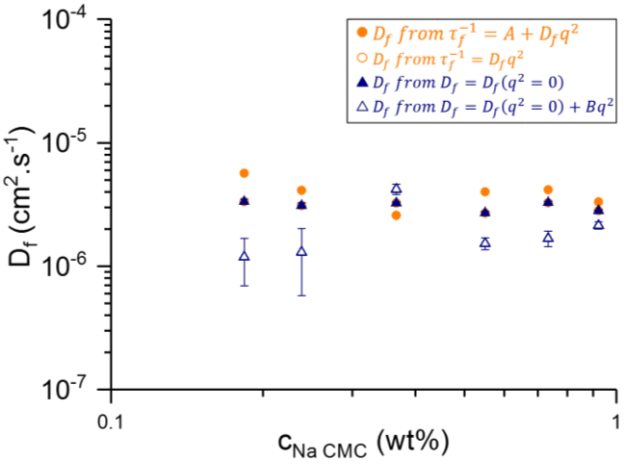


**Figure 7:** Fast mode diffusion coefficients as a function of Na CMC concentration. The calculation methods are explicitly shown in the SI (Figure S17).

*Slow mode*

The contribution of the slow mode to the total excess Rayleigh ratio $\Delta R_s$ (called slow mode amplitude by Sedlák)[63] is $q$-dependent, as shown in Figure S18, and is proportional to the Na CMC concentration. A $q$-dependence of $\Delta R_s$ has been observed for Na PSS in water without added salt[22] as well as in an organic solvent in the presence of salt.[65] The $q$- and $c_{Na\ CMC}$-concentration dependences of the slow relaxation time $\tau_s$ are shown in Figure 8. It is found that as the Na CMC concentration is increased, the relaxation time $\tau_s$ also increases. The $q$- and $c_{Na\ CMC}$-concentration dependences of the stretching exponent $\beta_s$ (see Eq. 5) are illustrated in the inset of Figure 8 for a few Na CMC concentrations. Within the accuracy of the measurements, $\beta_s$ is independent of Na CMC concentration, but decreases with $q$. Its value is around 0.7; which is in agreement with the value found by Dogsa *et al.*[14] for Na CMC solutions of smaller DS and $M_w$, as well as with values usually found for polyelectrolyte solutions whose slow mode is successfully fitted with a stretched exponential.[53,83]

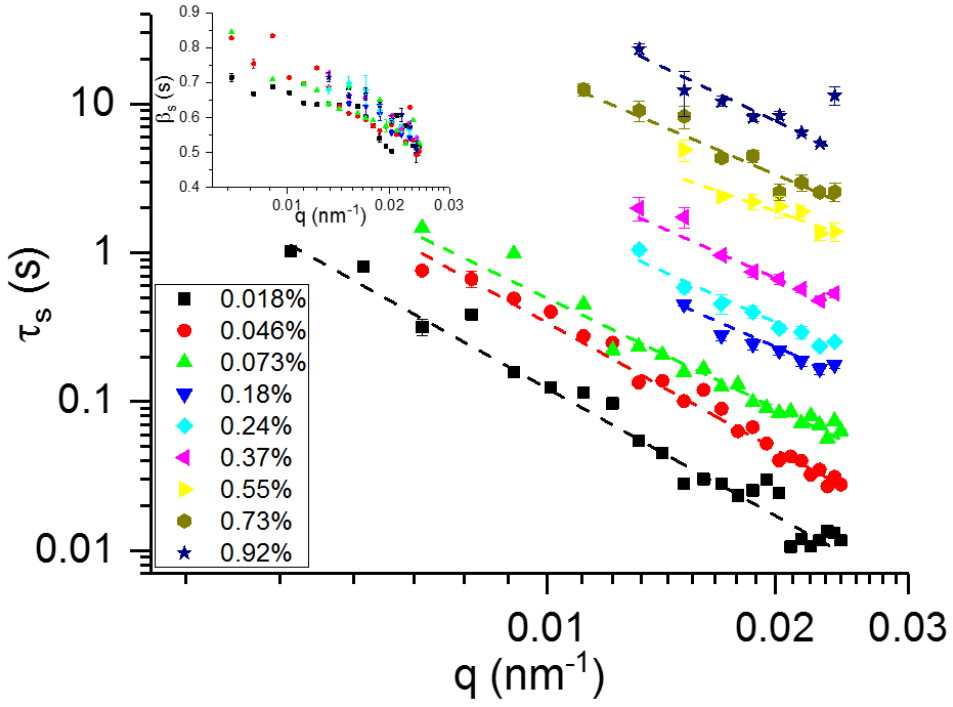


**Figure 8:** $q$- and $c_{Na\ CMC}$-dependence of the slow mode. Slow mode relaxation time $\tau_s$ as a function of the scattering vector $q$ for all studied concentrations ($c_{Na\ CMC}$ in *wt*%). For concentrations of 0.18 *wt*% Na CMC and above, DLS measurements could not be successfully performed at the lowest angles (corresponding to the lowest $q$ values) as the durations required to collect statistically reliable data allowed too many of the particulates to enter the scattering volume, thus providing unreliable data. Consequently, the data collected for these solutions cover a smaller $q$ range. Dashed lines are power law fits. The average exponent value across all concentrations is -2.4 ± 0.2. Exponent values are shown in Figure S19. Inset shows the stretching coefficient $\beta_s$ as a function of $q$, for a few Na CMC concentrations.

The relationship between the slow mode relaxation time and Na CMC concentration is also shown in Figure 9.A, which presents $\tau_s$ at 90° scattering angle as a function of $c_{Na\ CMC}$ across the studied range of concentrations, as well as in Figure S20 in the SI which shows the concentration dependence of $\tau_s$ at two other scattering angles. Figures 8, 9.A and Figure S20 all confirm that including the ultra-slow mode in the fits is successful in removing its influence on the $\tau_s$ values. Figure 9.A also compares $\tau_s(90°)$ with the specific viscosity $\eta_{sp}$ and shows that they exhibit a similar concentration dependence, suggesting that the slow mode is related to the viscosity of the solutions across the studied concentration range. A similar result was found by Esquenet and Buhler[53] for high molecular weight xanthan and hyaluronan samples (average molecular weights of $4.2 \times 10^6$ and $2 \times 10^6$ g/mol respectively) in 0.1 M NaCl. In our case, the $q$-dependence of the slow mode can be described using power laws, where the average value of power law exponents across all concentrations is -2.4 ± 0.2 (the exponent values for each studied concentrations are

given in Figure S19 within the SI). Similarly to the fast mode, the exponent is close to 2; thus suggesting that the slow mode is also related to a diffusive process. There is, however, a slight concentration dependence with greater values at low concentrations, likely due to the increased difficulty in determining $\tau_s$ for very dilute solutions and/or to the presence of additional relaxation contributions (*e.g.* relaxation contributions of internal modes). These effects are also illustrated in the data representation shown in Figure S21 within the SI.

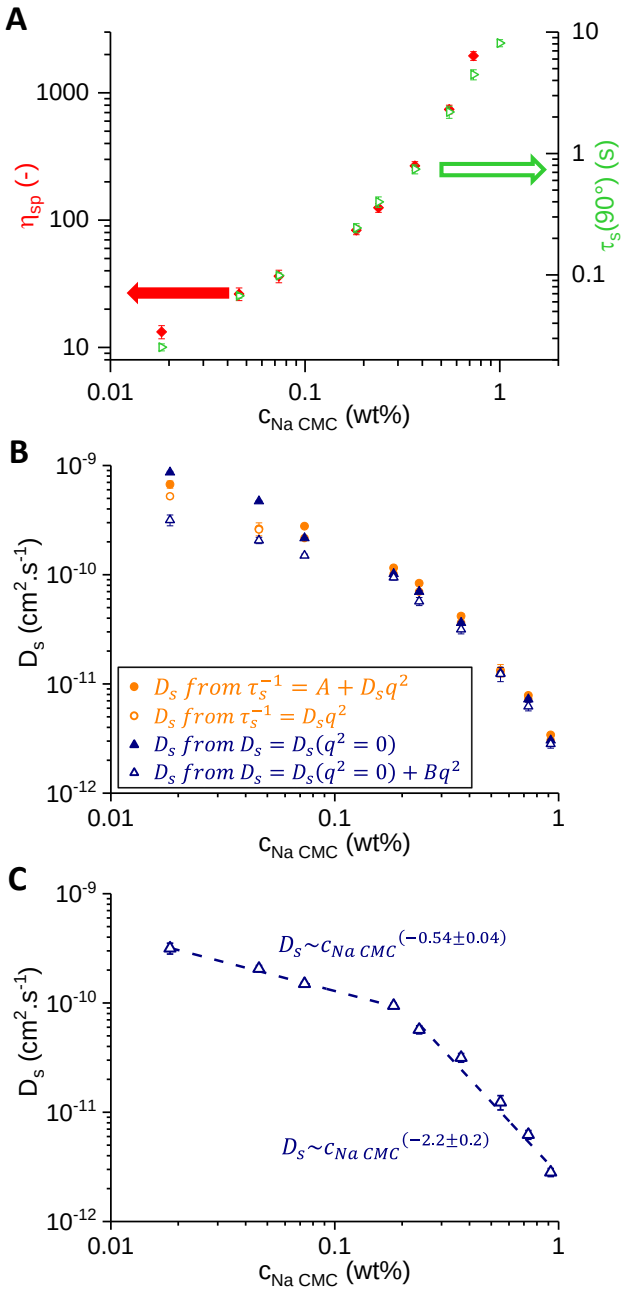


**Figure 9:** Polymer concentration dependences for the slow mode relaxation time $\tau_s$ and slow mode diffusion coefficient $D_s$. **A.** Concentration dependence of the slow mode relaxation time $\tau_s$ at 90° scattering angle and the specific viscosity. **B.** Concentration dependence of $D_s$ for $D_s$ values calculated with four methods (as shown for the fast mode). **C.** Concentration dependence of $D_s$, with the $D_s$ values retained for further calculations ($D_s$ values from $D_s = D_s(q^2 = 0) + Bq^2$). Dashed lines are the best power law fits of $D_s = f(c_{Na\ CMC})$.

The same methods as for the fast mode were used to calculate the diffusion coefficient $D_s$ of the slow mode (see previous subsection for more details). Values of $D_s$ obtained with the four methods

are shown in Figure 9.B. For the most concentrated solutions, the $D_s$ values are very close, regardless of the calculation method. For the three least concentrated solutions, the values are somewhat different from each other. This discrepancy is most likely due to the fact that the slow mode is not strictly linear in $q^2$ at these low concentrations (see Figures S21 and S22 illustrating the $D_s$ calculation methods for a low and a high Na CMC concentrations respectively) which is usually attributed to the large size of the domains and to their polydispersity.[22,55]

$D_s = f(c_{Na\ CMC})$ suggests a change in the concentration behavior for an intermediate concentration, where the behavior can be approximately described by power laws at both low and high concentrations, as shown in Figure 9.C which displays the values of $D_s$ obtained using Eq. 7. The equivalent graphs obtained for the three other calculation methods are shown in Figure S23 of the SI, where the fitting parameters for all four methods are reported in Table S2. This type of behavior has previously been observed in the literature for high molecular weight polyelectrolytes in salt-free solutions above $c^*$.[47,48] The power law exponent of the fit describing the low concentration region is -0.54 ± 0.04, which is in a similar range compared to the values of -0.35 and -0.7 obtained by Sedlák and co-workers obtained for Na PSS[47] and poly(methacrylic acid), respectively.[48] The power law exponent describing the high concentration region is -2.2 ± 0.2; which is much higher than the values of -0.83 and 1.4 found for the two previously cited polyelectrolytes.[47,48] It has however been shown that the value of the power law exponent $\upsilon$ of the relationship $D_s \sim c^{\nu}$ increases with the polymer molecular weight.[57]

The crossover concentration determined from the intercept of the two power laws for our system is ~ 0.21% (as determined from the fits shown in Figure 9.C; the values obtained using the other methods are similar and can be found in Table S2 of the SI; as for the crossover concentrations determined from rheology data (see Section 3.2), these concentrations are only estimates of where a change in behavior occurs). Sedlák and Amis[47] found a similar crossover concentration in Na PSS solutions. They also observed that this crossover concentration does not correspond to $c^{**}$ predicted by the version of the scaling laws for polyelectrolytes improved by Odijk.[47] The crossover concentration for our system is close to the entanglement concentration $c_e$ = 0.16%, as calculated using the scaling laws; so it is reasonable to assume that they both correspond to the onset of entanglements. This is in agreement with the previously observed similarity in the behavior of the specific viscosity and the slow mode relaxation time shown in Figure 9.A. The fact

that the change in concentration behavior of $D_s$ *vs* $c_{Na\ CMC}$ is not observed for low molecular weight polymers[47,48] is consistent with this hypothesis, since low molecular weight polymer chains are too short to be entangled.

Using the values of $D_s$ plotted in Figure 9.C (*i.e.* assuming the slow mode is diffusive), the apparent hydrodynamic radii $R_{H,app}$ of the domains were estimated using Eq. 8.

$$R_{H,app} = \frac{kT}{6\pi\eta D_s} \quad (8)$$

where $k$ is the Boltzmann constant, $T$ the temperature and $\eta$ the solution viscosity. The obtained values of $R_{H,app}$ are plotted in Figure S24 in the SI together with the estimated values of the apparent radii of gyration of the domains $R_{g,app}$ obtained from the Berry plots of the excess Rayleigh ratio associated with the slow mode $\Delta R_s$. Details on the determination of $R_{g,app}$ are provided in Section 4.6.3 of the SI. $R_{g,app}$ is relatively independent of the Na CMC concentration and an average value of 200 ± 20 nm is estimated across the studied range of concentrations. This value is of the same order of magnitude as the one obtained for a ~ 900,000 g/mol hyaluronan sample in 0.1 M NaCl.[53] $R_{g,app}$ has also been found to be independent of the polyelectrolyte concentration above $c^*$ for two hyaluronan samples of smaller $M_w$,[53] for PMPVP[49] and for chitosan in an electrolyte solution,[52] while they have been found to increase with the polyelectrolyte concentration for Na PSS.[23,55,86] It is worth noting that Buhler and Rinaudo[52] highlight the fact that $R_g$ is likely to increase with the polyelectrolyte concentration and to be larger than $R_{g,app}$. The values of $R_{H,app}$ in the present study are of the same order of magnitude as $R_{g,app}$. We find that the values decrease over the studied range of concentration; which is different from the results of Buhler and Rinaudo[52] who studied chitosan in the presence of a background electrolyte and found that $R_{H,app}$ instead increased with increasing chitosan concentration.

## 4. Conclusions

In this work, the behavior of Na CMC in aqueous solutions without added salt was investigated for a wide range of concentrations, using rheology and light scattering measurements.

For the studied concentration range, the concentration dependence of the specific viscosity could be described by the scaling theory for polyelectrolytes using a set of power laws. Three concentration regimes were identified: semi-dilute non-entangled, semi-dilute entangled and

concentrated. The so-determined power law exponents slightly differed from the theoretically predicted values but were consistent with those previously found for Na CMC. Alternatively, the data could be described using a simple empirical equation which links two power law behaviors only including one crossover concentration. The success of this approach suggests that only the semi-dilute non-entangled and entangled regimes are observed.

To further test this, Na CMC solutions covering the same concentration range were investigated using both SLS and DLS. The excess Rayleigh ratio, as determined from SLS, was found to vary linearly with Na CMC concentration. For all the studied solutions, it followed a power law relationship with the scattering wave vector $q$ and a power law exponent of $-2.36 \pm 0.05$, which was independent of the Na CMC concentration. Three relaxation modes were observed in DLS measurements. The two fastest modes were identified as the fast and slow relaxation modes commonly observed for polyelectrolytes. The third, and slowest mode, was attributed to poorly substituted undissolved cellulose fragments. As filtration (or centrifugation) did not sufficiently remove these fragments, and importantly did alter the solution behavior, both data collection and processing were adapted to account for the presence of this mode; we were thus able to perform the detailed LS characterization on the original Na CMC solutions, which are relevant for industrial applications. The diffusion coefficient $D_f$ of the fast relaxation mode was found to be concentration-independent and equal to $(3.1 \pm 0.2) \times 10^{-6}$ $cm^2.s^{-1}$. The relaxation time of the slow mode showed a similar crossover behavior to that found for the specific viscosity. Interestingly, no such change in behavior with Na CMC concentration was observed in the excess Rayleigh ratio, determined from static light scattering, suggesting that the origin of the observed behavior mainly originates from a change in dynamics. We note that the approach used in this study could be used also to investigate the behavior of Na CMC in the presence of other components commonly found in complex formulated products such as salts, sugars or solid particles, thus, acquiring detailed information which can guide the process and formulation design.

## Acknowledgments

This work was co-funded by the University of Leeds (University of Leeds 110 Anniversary Research Scholarship) and Procter and Gamble (P&G). We are grateful to the EPSRC (EP/J021156/1, EP/K005073/1, EP/J02113X/1) for supporting the LS spectrometer and related LS

work. Access to the Zeiss LSM700 microscope was provided by the Bio-imaging Facility of the Faculty of Biological Sciences of the University of Leeds. We also wish to thank Daniel Baker (University of Leeds) for his assistance regarding LS measurements, and Brian Jackson (University of Leeds) for his help with the microscope. We would like to thank the reviewers for their thoughtful suggestions.

**Supporting Information**

Supporting information available:

Figure S1: Examples of particulates observed in Na CMC solutions under the microscope; Figure S2: Small particulates observed in a 0.018 *wt*% Na CMC solution; Figure S3: Examples of particulates observed with a phase contrast microscope in microcrystalline cellulose suspensions; Figure S4: Examples of viscosity curves across the studied range of concentrations; Figure S5: Illustration of the methods used to calculate the crossover concentrations; Figure S6: Influence of measurement duration on the light scattering data collected for a 0.073 *wt*% Na CMC solution; Figure S7: Scattered intensity (or count rate) as a function of time for a 0.073 *wt*% Na CMC solution at $\theta = 30^{o}$ and for $\Delta t_{meas}$ = 10 min; Figure S8: Illustration of the method used to process the DLS data collected at an angle $\theta$; Figure S9: Measurement reproducibility and data processing for low Na CMC concentrations (0.073 *wt*%), intermediate Na CMC concentrations (0.37 *wt*%) and high Na CMC concentrations (0.55 *wt*%); Figure S10: Residuals of the fits shown in Figure S9; Figure S11: Comparison between the excess Rayleigh ratio $\Delta R$ values obtained during SLS and DLS measurements (*i.e.* short and long measurements, respectively); Figure S12: Refractive index as a function of Na CMC concentration; Figure S13: Determination of the excess Rayleigh ratio at $q^2 = 0$ for the 0.046 *wt*% Na CMC solution; Figure S14: $q$- and $c_{Na\ CMC}$-dependences of the ratio of the excess Rayleigh contributions of the slow and the fast modes $\Delta R_s/\Delta R_f$; Figure S15: Normalized intensity auto-correlation data over the full range of concentrations at three different scattering angles; Figure S16: $q$- and $c_{Na\ CMC}$ -dependences of the fast mode contribution to the excess Rayleigh ratio scattering; Figure S17: Illustration of the calculation of the fast mode diffusion coefficient $D_f$ with the 0.92 *wt*% Na CMC solution; Figure S18: $q$- and $c_{Na\ CMC}$-dependences of the slow mode contribution to the excess Rayleigh ratio scattering; Figure S19: Concentration-dependence of the power law exponents of $\tau_s = f(q)$;

Figure S20: Concentration and angle dependence of the slow mode relaxation time $\tau_s$; Figure S21: Illustration of the calculation of the slow mode diffusion coefficient Ds with the 0.046 *wt*% Na CMC solution; Figure S22: Illustration of the calculation of the slow mode diffusion coefficient Ds with the 0.18 *wt*% Na CMC solution; Figure S23: Concentration dependence of the slow mode diffusion coefficient $D_s$ calculated using four different methods; Figure S24: Apparent hydrodynamic radius $R_{H,app}$ and apparent radius of gyration $R_{g,app}$ of the domains as a function of Na CMC concentration.

Table S1: Fitting parameters obtained with the Carreau model for the data shown in Figure S4; Table S2: Fitting parameters of the power laws describing the behaviour of $D_s = f(c_{Na\ CMC})$ at low and high $c_{Na\ CMC}$ and shown in the plots A, B, C and D of Figure S23.

Additional details about the methods and further discussion of the data.

## Data statement

The article metadata, entitled Juliette Behra (2019): Characterization of Sodium Carboxymethyl Cellulose (Na CMC) Aqueous Solutions to Support Complex Product Formulation – a Rheology and Light Scattering Study – dataset. University of Leeds. [Dataset]. https://doi.org/10.5518/547, is available under a Creative Commons Attribution license (CC-BY) in the University of Leeds repository.

## References

(1) Lopez, C. G.; Rogers, S. E.; Colby, R. H.; Graham, P.; Cabral, J. T. Structure of Sodium Carboxymethyl Cellulose Aqueous Solutions: A SANS and Rheology Study. *J. Polym. Sci., Part B: Polym. Phys.* **2015,** *53*, 492-501.

(2) Joshi, G.; Naithani, S.; Varshney, V. K.; Bisht, S. S.; Rana, V.; Gupta, P. K. Synthesis and Characterization of Carboxymethyl Cellulose from Office Waste Paper: A Greener Approach Towards Waste Management. *Waste Manage.* **2015,** *38*, 33-40.

(3) Almlöf Ambjörnsson, H.; Schenzel, K.; Germgård, U. Carboxymethyl Cellulose Produced at Different Mercerization Conditions and Characterized by NIR FT Raman Spectroscopy in Combination with Multivariate Analytical Methods. *BioResources* **2013,** *8*, 1918-1932.

(4) Enebro, J.; Momcilovic, D.; Siika-aho, M.; Karlsson, S. A New Approach for Studying Correlations between the Chemical Structure and the Rheological Properties in Carboxymethyl Cellulose. *Biomacromolecules* **2007,** *8*, 3253-3257.

(5) Zhao, G. H.; Kapur, N.; Carlin, B.; Selinger, E.; Guthrie, J. T. Characterisation of the Interactive Properties of Microcrystalline Cellulose–Carboxymethyl Cellulose Hydrogels. *Int. J. Pharm. (Amsterdam, Neth.)* **2011,** *415*, 95-101.

(6) MarketsAndMarkets. Carboxymethyl Cellulose Market by Application (Food & Beverages, Pharmaceutical & Cosmetics, Oil & Gas, Paper, Detergents, and Others (Mining, Textiles Processing, Ceramics, Paints, Construction, and Adhesives)) - Trends & Forecasts to 2020 http://www.marketsandmarkets.com/Market-Reports/carboxymethyl-cellulose-market-16412328.html?gclid=EAIaIQobChMIyaiA976x1wIV1TLTCh34mwWpEAAYASAAEgLmvfD_BwE (accessed Nov 9, 2017).

(7) Transparency Market Research. Carboxymethyl Cellulose Market for Food and Beverages, Oil Drilling Fluids, Paper Processing, Personal Care, Paints & Adhesives, and Other End-Users - Global Industry Analysis, Size, Share, Growth, Trends and Forecast, 2013 - 2019. https://www.prnewswire.com/news-releases/carboxymethyl-cellulose-market-will-reach-us10398-million-by-2019-expanding-food-and-beverage-industry-to-drive-global-market-transparency-market-research-522683771.html (accessed Nov 9, 2017).

(8) Grand View Research. Carboxymethyl Cellulose Market Analysis by Application (Cosmetics & Pharmaceuticals, Food & Beverages, Oil & Gas, Paper & Board, Detergents), by Region, and Segment Forecasts, 2018 - 2025. https://www.grandviewresearch.com/industry-analysis/carboxymethyl-cellulose-cmc-market (accessed Sept 20, 2018).

(9) Global Market Insights. Carboxymethyl Cellulose Market Worth over $1.7bn by 2024. https://www.gminsights.com/pressrelease/carboxymethyl-cellulose-cmc-market (accessed Sept 20,2018).

(10) Arancibia, C.; Bayarri, S.; Costell, E. Effect of Hydrocolloid on Rheology and Microstructure of High-Protein Soy Desserts. *J. Food Sci. Technol. (New Delhi, India)* **2015,** *52*, 6435-6444.

(11) Ho Tan Tai, L., Liquid Detergents. In *Formulating Detergents and Personal Care Products - a Guide to Product Development*, AOCS Press: Champaign, 2000; pp 156-173.

(12) Pader, M., Dentifrice Rheology. In *Rheological Properties of Cosmetics and Toiletries.*, Laba, D., Ed. CRC Press: New-York, 1993; pp 247-273.

(13) Arinaitwe, E.; Pawlik, M. Dilute Solution Properties of Carboxymethyl Celluloses of Various Molecular Weights and Degrees of Substitution. *Carbohydr. Polym.* **2014,** *99*, 423-431.

(14) Dogsa, I.; Tomšič, M.; Orehek, J.; Benigar, E.; Jamnik, A.; Stopar, D. Amorphous Supramolecular Structure of Carboxymethyl Cellulose in Aqueous Solution at Different pH Values as Determined by Rheology, Small Angle X-Ray and Light Scattering. *Carbohydr. Polym.* **2014,** *111*, 492-504.

(15) Lopez, C. G.; Colby, R. H.; Cabral, J. T. Electrostatic and Hydrophobic Interactions in NaCMC Aqueous Solutions: Effect of Degree of Substitution. *Macromolecules* **2018,** *51*, 3165-3175.

(16) Lopez, C. G.; Colby, R. H.; Graham, P.; Cabral, J. T. Viscosity and Scaling of Semiflexible Polyelectrolyte NaCMC in Aqueous Salt Solutions. *Macromolecules* **2017,** *50*, 332-338.

(17) Hulskotter, F.; Scialla, S.; Loughnane, B. J.; Brooker, A. T.; Ure, C.; Ebert, S. R.; Ludolph, B.; Wigbers, C.; Maas, S.; Boeckh, D.; Eidamshaus, C. Cleaning Compositions Containing a Polyetheramine, a Soil Release Polymer, and a Carboxymethylcellulose. US 9,193,939 B2 Nov 24, 2015.

(18) Nicolae, A.; Radu, G.-L.; Belc, N. Effect of Sodium Carboxymethyl Cellulose on Gluten-Free Dough Rheology. *J. Food Eng.* **2016,** *168*, 16-19.

(19) Savadkoohi, S.; Farahnaky, A. Small Deformation Viscoelastic and Thermal Behaviours of Pomegranate Seed Pips CMC Gels. *J. Food Sci. Technol. (New Delhi, India)* **2014,** *52*, 1-10.

(20) Savadkoohi, S.; Mesbahi, G.; Niakousari, M.; Farahnaky, A. A New Study on the Steady Shear Flow, Thermal and Functional Properties of Beet Pulp Carboxymethyl Cellulose. *J. Food Process. Preserv.* **2014,** *38*, 2117-2128.

(21) Dobrynin, A. V.; Rubinstein, M. Theory of Polyelectrolytes in Solutions and at Surfaces. *Prog. Polym. Sci.* **2005,** *30*, 1049-1118.

(22) Sedlák, M. What Can Be Seen by Static and Dynamic Light Scattering in Polyelectrolyte Solutions and Mixtures? *Langmuir* **1999,** *15*, 4045-4051.

(23) Sedlák, M. Domain Structure of Polyelectrolyte Solutions: Is It Real? *Macromolecules* **1993,** *26*, 1158-1162.

(24) Sedlák, M. The Ionic Strength Dependence of the Structure and Dynamics of Polyelectrolyte Solutions as Seen by Light Scattering: The Slow Mode Dilemma. *J. Chem. Phys.* **1996,** *105*, 10123-10133.

(25) Cheng, H. N.; Takai, M.; Ekong, E. A. Rheology of Carboxymethylcellulose Made from Bacterial Cellulose. *Macromol. Symp.* **1999,** *140*, 145-153.

(26) Eremeeva, T. E.; Bykova, T. O. SEC of Mono-Carboxymethyl Cellulose (CMC) in a Wide Range of pH; Mark–Houwink Constants. *Carbohydr. Polym.* **1998,** *36*, 319-326.

(27) Kamide, K.; Okajima, K.; Kowsaka, K.; Matsui, T.; Nomura, S.; Hikichi, K. Effect of the Distribution of Substitution of the Sodium Salt of Carboxymethylcellulose on its Absorbency toward Aqueous Liquid. *Polym. J. (Tokyo, Jpn.)* **1985,** *17*, 909-918.

(28) Barba, C.; Montané, D.; Rinaudo, M.; Farriol, X. Synthesis and Characterization of Carboxymethylcelluloses (CMC) from Non-Wood Fibers I. Accessibility of Cellulose Fibers and CMC Synthesis. *Cellulose* **2002,** *9*, 319-326.

(29) Jardeby, K.; Germgård, U.; Kreutz, B.; Heinze, T.; Heinze, U.; Lennholm, H. Effect of Pulp Composition on the Characteristics of Residuals in CMC Made from such Pulps. *Cellulose* **2005,** *12*, 385-393.

(30) Kulicke, W.-M.; Kull, A. H.; Kull, W.; Thielking, H.; Engelhardt, J.; Pannek, J.-B. Characterization of Aqueous Carboxymethylcellulose Solutions in Terms of their Molecular Structure and its Influence on Rheological Behaviour. *Polymer* **1996,** *37*, 2723-2731.

(31) Kästner, U.; Hoffmann, H.; Dönges, R.; Hilbig, J. Structure and Solution Properties of Sodium Carboxymethyl Cellulose. *Colloids Surf., A* **1997,** *123–124*, 307-328.

(32) Yang, X.; Zhu, W. Viscosity Properties of Sodium Carboxymethylcellulose Solutions. *Cellulose* **2007,** *14*, 409-417.

(33) Francis, P. S. Solution Properties of Water-Soluble Polymers. I. Control of Aggregation of Sodium Carboxymethylcellulose (CMC) by Choice of Solvent and/or Electrolyte. *J. Appl. Polym. Sci.* **1961,** *5*, 261-270.

(34) Cancela, M. A.; Álvarez, E.; Maceiras, R. Effects of Temperature and Concentration on Carboxymethylcellulose with Sucrose Rheology. *J. Food Eng.* **2005,** *71*, 419-424.

(35) Guillot, S.; Delsanti, M.; Désert, S.; Langevin, D. Surfactant-Induced Collapse of Polymer Chains and Monodisperse Growth of Aggregates near the Precipitation Boundary in Carboxymethylcellulose−DTAB Aqueous Solutions. *Langmuir* **2003,** *19*, 230-237.

(36) Komorowska, P.; Różańska, S.; Różański, J. Effect of the Degree of Substitution on the Rheology of Sodium Carboxymethylcellulose Solutions in Propylene Glycol/Water Mixtures. *Cellulose* **2017,** *24*, 4151-4162.

(37) Okatova, O. V.; Lavrenko, P. N.; Dautzenberg, H.; Filipp, B. N.; Tsvetkov, V. N. Polyelectrolyte Effects in Diffusion and Viscosity Phenomena in Water-Cadoxene Solutions of Carboxymethylcellulose. *Polym. Sci. U.S.S.R.* **1990,** *32*, 533-539.

(38) Waring, M. J.; Parsons, D. Physico-Chemical Characterisation of Carboxymethylated Spun Cellulose Fibres. *Biomaterials* **2001,** *22*, 903-912.

(39) Arık Kibar, E. A.; Us, F. Thermal, Mechanical and Water Adsorption Properties of Corn Starch–Carboxymethylcellulose/Methylcellulose Biodegradable Films. *J. Food Eng.* **2013,** *114*, 123-131.

(40) Li, W.; Sun, B.; Wu, P. Study on Hydrogen Bonds of Carboxymethyl Cellulose Sodium Film with Two-Dimensional Correlation Infrared Spectroscopy. *Carbohydr. Polym.* **2009,** *78*, 454-461.

(41) Mutalik, V.; Manjeshwar, L. S.; Wali, A.; Sairam, M.; Sreedhar, B.; Raju, K. V. S. N.; Aminabhavi, T. M. Aqueous-Solution and Solid-Film Properties of Poly(Vinyl Alcohol), Poly(Vinyl Pyrrolidone), Gelatin, Starch, and Carboxymethylcellulose Polymers. *J. Appl. Polym. Sci.* **2007,** *106*, 765-774.

(42) Brown, W.; Henley, D. Studies on Cellulose Derivatives. Part IV. The Configuration of the Polyelectrolyte Sodium Carboxymethyl Cellulose in Aqueous Sodium Chloride Solutions. *Makromol. Chem.* **1964,** *79*, 68-88.

(43) Schneider, N. S.; Doty, P. Macro-Ions. IV. The Ionic Strength Dependence of the Molecular Properties of Sodium Carboxymethylcellulose. *J. Phys. Chem.* **1954,** *58*, 762-769.

(44) Trap, H. J. L.; Hermans, J. J. Light-Scattering by Polymethacrylic Acid and Carboxymethylcellulose in Various Solvents. *J. Phys. Chem.* **1954,** *58*, 757-761.

(45) Hoogendam, C. W.; de Keizer, A.; Cohen Stuart, M. A.; Bijsterbosch, B. H.; Smit, J. A. M.; van Dijk, J. A. P. P.; van der Horst, P. M.; Batelaan, J. G. Persistence Length of Carboxymethyl Cellulose as Evaluated from Size Exclusion Chromatography and Potentiometric Titrations. *Macromolecules* **1998,** *31*, 6297-6309.

(46) Lopez, C. G.; Richtering, W. Influence of Divalent Counterions on the Solution Rheology and Supramolecular Aggregation of Carboxymethyl Cellulose. *Cellulose* [Online early access]. DOI: 10.1007/s10570-018-2158-8. Published Online: Dec 10, 2018. https://link.springer.com/article/10.1007/s10570-018-2158-8 (accessed Jan 31, 2019).

(47) Sedlák, M.; Amis, E. J. Concentration and Molecular Weight Regime Diagram of Salt-Free Polyelectrolyte Solutions as Studied by Light Scattering. *J. Chem. Phys.* **1992,** *96*, 826-834.

(48) Sedlák, M.; Koňák, Č.; Štěpánek, P.; Jakeš, J. Semidilute Solutions of Poly(Methacrylic Acid) in the Absence of Salt: Dynamic Light-Scattering Study. *Polymer* **1987,** *28*, 873-880.

(49) Ermi, B. D.; Amis, E. J. Domain Structures in Low Ionic Strength Polyelectrolyte Solutions. *Macromolecules* **1998,** *31*, 7378-7384.

(50) Borsali, R.; Nguyen, H.; Pecora, R. Small-Angle Neutron Scattering and Dynamic Light Scattering from a Polyelectrolyte Solution: DNA. *Macromolecules* **1998,** *31*, 1548-1555.

(51) Wissenburg, P.; Odijk, T.; Cirkel, P.; Mandel, M. Multimolecular Aggregation of Mononucleosomal DNA in Concentrated Isotropic Solutions. *Macromolecules* **1995,** *28*, 2315-2328.

(52) Buhler, E.; Rinaudo, M. Structural and Dynamical Properties of Semirigid Polyelectrolyte Solutions: A Light-Scattering Study. *Macromolecules* **2000,** *33*, 2098-2106.

(53) Esquenet, C.; Buhler, E. Aggregation Behavior in Semidilute Rigid and Semirigid Polysaccharide Solutions. *Macromolecules* **2002,** *35*, 3708-3716.

(54) Cao, Z.; Zhang, G. Insight into Dynamics of Polyelectrolyte Chains in Salt-Free Solutions by Laser Light Scattering and Analytical Ultracentrifugation. *Polymer* **2014,** *55*, 6789-6794.

(55) Förster, S.; Schmidt, M.; Antonietti, M. Static and Dynamic Light Scattering by Aqueous Polyelectrolyte Solutions: Effect of Molecular Weight, Charge Density and Added Salt. *Polymer* **1990,** *31*, 781-792.

(56) Schmidt, M. Static and Dynamic Light Scattering by an Aqueous Polyelectrolyte Solution without Added Salt: Quaternized Poly(2-Vinylpyridine). *Makromol. Chem., Rapid Commun.* **1989,** *10*, 89-96.

(57) Sedlák, M.; Amis, E. J. Dynamics of Moderately Concentrated Salt-Free Polyelectrolyte Solutions: Molecular Weight Dependence. *J. Chem. Phys.* **1992,** *96*, 817-825.

(58) Nierling, W.; Nordmeier, E. Studies on Polyelectrolyte Solutions VII. Fast, Heterogeneous, and Slow Diffusion Modes of Poly(Diallyl-*N*,*N*-Dimethylammonium Chloride) in Aqueous Alcoholic Salt Solvents. *Polym. J. (Tokyo, Jpn.)* **1997,** *29*, 795-806.

(59) Topp, A.; Belkoura, L.; Woermann, D. Effect of Charge Density on the Dynamic Behavior of Polyelectrolytes in Aqueous Solution. *Macromolecules* **1996,** *29*, 5392-5397.

(60) Sedlák, M. Generation of Multimacroion Domains in Polyelectrolyte Solutions by Change of Ionic Strength or pH (Macroion Charge). *J. Chem. Phys.* **2002,** *116*, 5256-5262.

(61) Zhou, K.; Li, J.; Lu, Y.; Zhang, G.; Xie, Z.; Wu, C. Re-Examination of Dynamics of Polyeletrolytes in Salt-Free Dilute Solutions by Designing and Using a Novel Neutral−Charged−Neutral Reversible Polymer. *Macromolecules* **2009,** *42*, 7146-7154.

(62) Ghosh, S.; Peitzsch, R. M.; Reed, W. F. Aggregates and Other Particles as the Origin of the "Extraordinary" Diffusional Phase in Polyelectrolyte Solutions. *Biopolymers* **1992,** *32*, 1105-1122.

(63) Sedlák, M. Mechanical Properties and Stability of Multimacroion Domains in Polyelectrolyte Solutions. *J. Chem. Phys.* **2002,** *116*, 5236-5245.

(64) Cong, R.; Temyanko, E.; Russo, P. S.; Edwin, N.; Uppu, R. M. Dynamics of Poly(Styrenesulfonate) Sodium Salt in Aqueous Solution. *Macromolecules* **2006,** *39*, 731-739.

(65) Sehgal, A.; Seery, T. A. P. The Ordinary−Extraordinary Transition Revisited: A Model Polyelectrolyte in a Highly Polar Organic Solvent. *Macromolecules* **1998,** *31*, 7340-7346.

(66) Ermi, B. D.; Amis, E. J. Influence of Backbone Solvation on Small Angle Neutron Scattering from Polyelectrolyte Solutions. *Macromolecules* **1997,** *30*, 6937-6942.

(67) Sedlák, M. Long-Time Stability of Multimacroion Domains in Polyelectrolyte Solutions. *J. Chem. Phys.* **2002,** *116*, 5246-5255.

(68) ASTM D1439-03(2008), Standard Test Methods for Sodium Carboxymethylcellulose. In *Annual Book of ASTM Standards*, ASTM International: Philadelphia, 2010; Vol. 6.03, pp 245-250.

(69) Lohmander, U.; Strömberg, R. Non-Newtonian Flow of Dilute Sodium Carboxymethyl Cellulose Solutions at Different Ionic Strengths and of Dilute Solutions of Cellulose Nitrate and Polystyrene in Moderately Viscous Solvents Studied by Capillary Viscometry · Experimental Results. *Makromol. Chem.* **1964,** *72*, 143-158.

(70) Höppler, F. Rheometrie Und Kolloidik Des Systems Natriumzelluloseglykolat—Wasser. *Kolloid-Z.* **1942,** *98*, 348-358.

(71) Jardeby, K.; Germgård, U.; Kreutz, B.; Heinze, T.; Heinze, U.; Lennholm, H. The Influence of Fibre Wall Thickness on the Undissolved Residuals in CMC Solutions. *Cellulose* **2005,** *12*, 167-175.

(72) Jardeby, K.; Lennholm, H.; Germgård, U. Characterisation of the Undissolved Residuals in CMC-Solutions. *Cellulose* **2004,** *11*, 195-202.

(73) Siqueira, E. J.; Brochier Salon, M. C.; Mauret, E. The Effects of Sodium Chloride (Nacl) and Residues of Cellulosic Fibres Derived from Sodium Carboxymethylcellulose (NaCMC) Synthesis on Thermal and Mechanical Properties of CMC Films. *Ind. Crops Prod.* **2015,** *72*, 87-96.

(74) Rubinstein, M.; Colby, R. H., *Polymer Physics*. Oxford University Press: New-York, 2003.

(75) Strobl, G., *The Physics of Polymers. Concepts for Understanding their Structures and Behavior*. 3rd ed.; Springer: Berlin, 2007, pp. 70, 82-83, 88, 93-95.

(76) Rubinstein, M.; Colby, R. H.; Dobrynin, A. V. Dynamics of Semidilute Polyelectrolyte Solutions. *Phys. Rev. Lett.* **1994,** *73*, 2776-2779.

(77) Colby, R. Structure and Linear Viscoelasticity of Flexible Polymer Solutions: Comparison of Polyelectrolyte and Neutral Polymer Solutions. *Rheol. Acta* **2010,** *49*, 425-442.

(78) Dou, S.; Colby, R. H. Charge Density Effects in Salt-Free Polyelectrolyte Solution Rheology. *J. Polym. Sci., Part B: Polym. Phys.* **2006,** *44*, 2001-2013.

(79) Dobrynin, A. V.; Colby, R. H.; Rubinstein, M. Scaling Theory of Polyelectrolyte Solutions. *Macromolecules* **1995,** *28*, 1859-1871.

(80) Truzzolillo, D.; Bordi, F.; Cametti, C.; Sennato, S. Counterion Condensation of Differently Flexible Polyelectrolytes in Aqueous Solutions in the Dilute and Semidilute Regime. *Phys. Rev. E* **2009,** *79*, 011804.

(81) Truzzolillo, D.; Cametti, C.; Sennato, S. Dielectric Properties of Differently Flexible Polyions: A Scaling Approach. *Phys. Chem. Chem. Phys.* **2009,** *11*, 1780-1786.

(82) Schärtl, W., *Light Scattering from Polymer Solutions and Nanoparticle Dispersions*. Springer: Berlin, 2007.

(83) Ioan, C. E.; Aberle, T.; Burchard, W. Light Scattering and Viscosity Behavior of Dextran in Semidilute Solution. *Macromolecules* **2001,** *34*, 326-336.

(84) Vaccaro, A. Light Scattering: Fundamentals. http://www.lsinstruments.ch/technology/slide_shows/ (accessed Nov 1, 2017).

(85) Zhang, Y.; Douglas, J. F.; Ermi, B. D.; Amis, E. J. Influence of Counterion Valency on the Scattering Properties of Highly Charged Polyelectrolyte Solutions. *J. Chem. Phys.* **2001,** *114*, 3299-3313.

(86) Tanahatoe, J. J.; Kuil, M. E. Light Scattering on Semidilute Polyelectrolyte Solutions: Molar Mass and Polyelectrolyte Concentration Dependence. *J. Phys. Chem. B* **1997,** *101*, 9233-9239.

(87) Némethy, G.; Scheraga, H. A. Structure of Water and Hydrophobic Bonding in Proteins. IV. The Thermodynamic Properties of Liquid Deuterium Oxide. *J. Chem. Phys.* **1964,** *41*, 680-689.

(88) Gittings, M. R.; Cipelletti, L.; Trappe, V.; Weitz, D. A.; In, M.; Marques, C. Structure of Guar in Solutions of $H_2O$ and $D_2O$: An Ultra-Small-Angle Light-Scattering Study. *J. Phys. Chem. B* **2000,** *104*, 4381-4386.

(89) Burchard, W., Light Scattering. In *Physical Techniques for the Study of Food Biopolymers*, Ross-Murphy, S. B., Ed. Blackie Academic & Professional: London, 1994; pp 151-213.

(90) Ermi, B. D.; Amis, E. J. Model Solutions for Studies of Salt-Free Polyelectrolytes. *Macromolecules* **1996,** *29*, 2701-2703.

## Table of Contents Graphics